AVO analysis of 3-D seismic data at Cold Lake

J. Helen Isaac and Don C. Lawton

ABSTRACT

Laterally and temporally variable amplitude anomalies are observed on 3-D timelapse seismic volumes over a heavy oil field which is undergoing cyclical steam stimulation. These timelapse seismic data were acquired during production and steam injection cycles. The amplitude anomalies seen in the stacked data are interpreted to be caused by gas-saturated zones in the 1990 data (production) and by steamed zones in the 1992 data (injection). Forward modelling predicts that a measurable increase in amplitude should occur in data acquired in steam- or gas-saturated zones. The modelling also shows that the farthest source-receiver offset should be restricted to less than 500 m and that, to avoid ambiguous results, offsets in the 1990 data, where partially gas-saturated zones are under analysis, should be restricted to less than 250 m.

Amplitude anomalies were selected from the two stacked 3-D data volumes to investigate intervals interpreted to be steam- or gas-saturated. For the majority of the supergathers examined, the AVO values obtained agree with the interpretation of the stacked data amplitude anomalies. Analysis of selected supergathers along a 3-C *P-P* line, to detect partial gas-saturation at the top of the reservoir, resulted in negative AVO values for all the gathers away from the injection wells and positive AVO values for most of the gathers at the well locations. Crossplots of AVO value against *Vp/Vs* from the 3-C line and against scaled average amplitude from the corresponding 3-D line indicate that a negative AVO value with *Vp/Vs* over 2.2 or with negative average amplitude can be used to classify that point as lying in cold reservoir with a high degree of confidence.

INTRODUCTION

Seismic monitoring methods are employed at Cold Lake, Alberta, where the reservoir is undergoing cyclical steam stimulation to reduce the viscosity of the bitumen contained in the sands (from 100 Pa.s at 30˚C to .006 Pa.s at 200˚C. Steam is injected into the reservoir at a fluid pressures up to 8 MPa - 10 MPa and at temperatures as high as 315˚C. The cold reservoir temperature is 15˚C, whereas reservoir temperatures during production vary from 120˚C - 200˚C. At Cold Lake, the bitumen has to be heated to at least 75˚C before it will flow. The bitumen is contained in the Lower Cretaceous Clearwater sands, which are unconsolidated and have an average porosity of 32% in the study area. At Imperial Oil's D3 pad, timelapse 3-D seismic data were acquired in 1990, during a production cycle, and in 1992, during a steam injection cycle. At the nearby AABBW pads, experimental timelapse converted-wave data were acquired in 1993 and 1994. Processing and interpretation of both the 3-D and converted-wave data have been discussed in previous CREWES Research Reports (Isaac and Lawton, 1993; 1994; 1995).

Selected portions of three of the Cold Lake seismic data sets (1990 3-D, 1992 3-D and 1993 3-C) were analysed for amplitude variations with offsets. The objective of this study was to determine whether amplitude variation with offset (AVO) analysis could confirm the interpretation of low velocity intervals as determined from amplitude anomalies delineated on the 3-D data volumes. Amplitude anomalies observed in the 1990 3-D data are interpreted to be caused by partial gas-saturation while anomalies in the 1992 data are interpreted to be caused by the presence of steam. Tsingas and

Kanasewich (1991) employed amplitude versus angle analysis of 2-D seismic data over a steam injection location at Cold Lake. They showed that the lateral extent of steam invaded zones may be established by observation of the variations in reflection amplitude with angle.

A *P-P* line from the 1993 3-C survey was also analysed. Few significant amplitude anomalies are seen within the reservoir interval but the character of the Clearwater event varies across the line. Since this event is only seen clearly on *P-P* seismic data at the AABBW pads when gas exists at the top of the reservoir (J. Eastwood, *pers. comm.*), the AVO analysis was designed to investigate potential gas-charged intervals. It was not possible to analyse the converted-wave data as they had not been processed specifically to retain true relative amplitudes. Also, the converted-wave data were *f-k* and *f-x* filtered to enhance horizontal events and to improve the signal to noise ratio.

AMPLITUDE ANALYSIS

Amplitude anomalies

Figure 1 shows corresponding crosslines extracted from the two 3-D data volumes. The Clearwater reservoir extends from about 0.405 s to 0.455 s. In Figure 1b (the 1992 line) a high amplitude event can be seen on inline traces 34 to 40 at a time of 0.435 s. This event is not seen on the 1990 line (Figure 1a) and its arrival time corresponds to the depth of the perforations in the injection wells. This high amplitude anomaly is situated near the location of injection well D3-8 at inline 35 and is interpreted to be due to the presence of steam in the reservoir during the acquisition of the 1992 survey.

The presence of a high amplitude trough on the 1990 line (Figure 1a) at about 0.425 s over traces 40 to 60, which is absent on the 1992 line, also indicates a temporal change in reservoir conditions. It is interpreted to be due to the localised presence of a gas-saturated zone. These zones were present during the production cycle in 1990 but absent in 1992, when pore fluid pressures were too high for the existence of gas, except in very thin zones (Eastwood et al., 1994).

The Chiburis method of AVO analysis

The method of data analysis used was that of Chiburis (1984; 1993), which normalises the amplitudes of target and reference horizons to eliminate or greatly reduce amplitude effects from causes other than offset. In Chiburis's method of AVO analysis, seismic amplitudes are picked interactively along both the target horizon and a reference horizon (over which no distinctive offset-dependent amplitude effects should be expected). The maximum amplitudes of the target event, $T(x)$, and of the reference event, $W(x)$, are measured at each offset, x, within a gather. The target to reference amplitude ratios are normalised:

$$R(x) = \{T(x) / Ta\} / \{W(x) / Wa\} \qquad (1)$$

where $R(x)$ is the amplitude ratio at offset x and Ta and Wa are the average amplitudes of the target and reference horizons, respectively. Each ratio is further modified:

$$\text{If } R(x) > 1, \quad R(x) = 2 - 1/R(x) \tag{2}$$

which has the result of bounding the ratios between 0 and 2. This ratio is known as the conditioned amplitude ratio. A curve of the form $y = B + Ax^2$ is fitted to the plot of conditioned amplitude ratio against offset and, finally, the AVO difference (relative to zero-offset) for the gather is formed by:

$$\text{AVO difference} = B/A * N^2 \tag{3}$$

where N is the number of traces in the gather. Since N is a scaling factor, it is arbitrary and could equally be the farthest offset. Chiburis refers to this AVO difference as "AVO", for simplicity.

AVO MODELLING OF COLD LAKE DATA

Model and synthetic seismic gathers

Before analysing the seismic data for AVO effects, several models were created to simulate the interpreted conditions of steam- and gas-saturated intervals within the reservoir. It was predicted that the modelled AVO responses would indicate that measurable AVO results could be extracted from the real data. If the low velocity intervals behaved in the same way as Class 3 gas sands (Rutherford and Williams, 1989), then it is possible that a significant increase in amplitudes with offset might not be seen. Small increases in amplitude on the modelled data might imply that such changes would be hard to measure on real data because of interfering noise. It was also anticipated that the modelling would allow confirmation of the interpretation that anomalies on the stacked seismic data are caused by low velocity zones.

For the generation of synthetic seismic traces, it is necessary to select a wavelet to be convolved with the generated acoustic impedances. In the modelling presented, both Ormsby bandpass and extracted wavelets were used. The first extracted wavelet (1) came from the 1990 3-D seismic data. It was 100 ms long and was composed of a primary event followed by a secondary one 25 ms later. It was thought that this second event could be the result of a ghost reflection from the ground surface, 10 m shallower than the geophones. The second extracted wavelet (2) came from the 1993 *P-P* data, at the location of well BB27. It was considered that wavelet (1) was not suitable for use in the modelling of low velocity zones in the 1993 *P-P* data because the geophones for the 3-D survey were buried, while those for the 3-C survey were at the surface. The choice of wavelet will be seen to affect the modelled AVO response and influence the range of offsets to be included in the analyses.

Several log models were created to observe the calculated effects on seismic amplitudes of introducing gas-saturated or steamed zones into the reservoir. The logs edited were the *P*-wave and *S*-wave dipole logs from well BB13a and the *P*-wave log from well BB27 for the shallow section. Well BB13a encountered a 15 m thick gas-charged interval at the top of the Clearwater Formation, which is apparent as a low velocity (1950 m/s) zone on the *P*-wave sonic log.

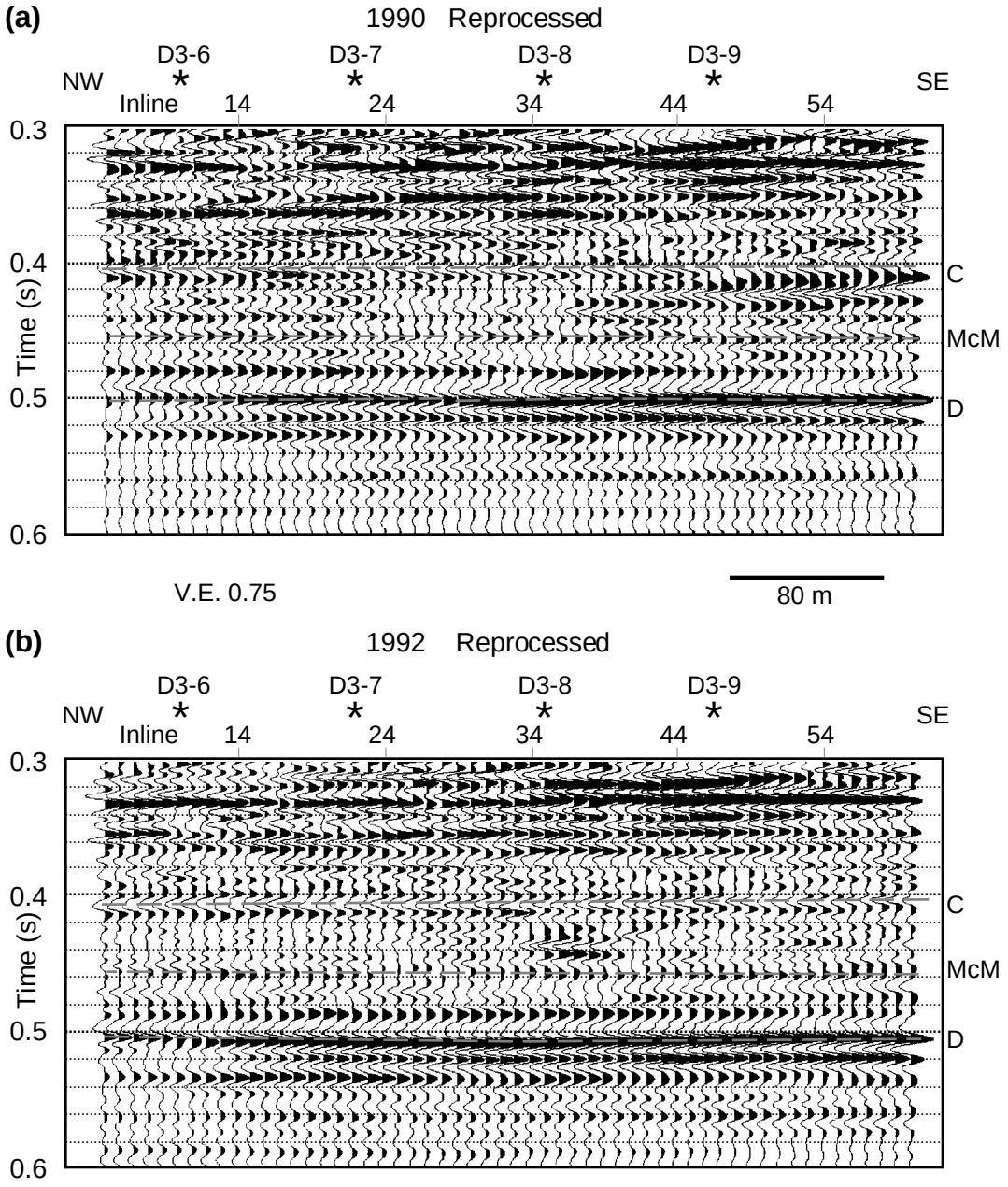

Fig. 1. Seismic lines taken from the centre of the **(a)** 1990 and **(b)** 1992 3-D volumes. The projected locations of steam injection wells are indicated by asterisks. "C" denotes the top of the Clearwater Fm., "McM" the top of the McMurray Fm. and "D" the top of the Devonian section.

Hampson-Russell AVO software was used to generate synthetic seismic offset gathers and stacked gathers for the original logs and the modifications, which were intended to simulate various reservoir conditions. Each of the two sonic logs was blocked into the same irregular intervals of constant velocity. Constant density values were input for each blocked interval within the zone of interest. The values were obtained from logs acquired at the D3 pad and from physical parameters of the Clearwater sands (Eastwood, 1993). Density values used were as follows: Grand Rapids Formation, 2150 kg/m^3; cold Clearwater Formation, 2100 kg/m^3; gas-charged interval, 2060 kg/m^3; steamed interval, 2065 kg/m^3 and McMurray Formation, 2250 kg/m^3. Poisson's ratio within each blocked interval was calculated automatically from the *P*- and *S*-wave velocities and density. Six situations were modelled:

(a) A gas-charged zone at the top of the reservoir. This was interpreted from the original logs.

(b) A gas-charged zone beneath a tight streak near the top of the reservoir. This model was designed to simulate the situation thought to exist in places at the D3 pad in 1990. High amplitude events on the 1990 seismic data at about 0.425 s (Figure 1a) were interpreted to be gas-saturated zones - an interpretation supported by the inversion study (Isaac and Lawton, 1994).

(c) No gas present at the top of the reservoir.

(d) A 6 m steamed zone present at the depth of the perforations. High amplitude anomalies seen on the 1992 seismic data at a time of about 0.437 s (Figure 1b) were interpreted to be steam-saturated zones.

(e) An 18 m steamed zone at the base of the reservoir. The thickness of the steamed zone was increased to observe the effects of tuning caused by the thinner zone.

(f) No steam present at the perforation depth.

Figure 2 shows the results for case (a), a 15 m thick gas-saturated zone at the top of the reservoir. Plotted are the original input logs overlain with the blocked logs, Poisson's ratio, a gather showing offsets up to 600 m and the stacked trace of these offsets (with NMO stretch muting applied; repeated five times). The gas interval is annotated next to the *P*-wave sonic log. The time scale for the seismic traces has been adjusted to reflect the arrival times of the modelled events on the actual seismic data from the D3 pad. The top of the gas-charged interval correlates to the trough at about 0.408 s and the base of the zone to the peak at 0.424 s. The interval is thick enough so that there are no adverse tuning effects between the top and base of the interval. An Ormsby bandpass wavelet (10/15-100/120 Hz) was used in the generation of these seismic traces.

Case (d) results (a 6 m thick steamed zone at the depth of the perforations) are presented in Figure 3 in the same way as for case (a). The *P*-wave sonic log was edited to simulate a steamed zone from 457 to 463 m with an interval velocity of 1750 m/s. The *S*-wave sonic log was also edited to a value of 1190 m/s. The top of the steamed interval is represented by the trough at 0.438 s which corresponds to the arrival time of the anomalies observed on the 1992 3-D seismic data. The base of the zone corresponds to the peak at 0.445 s but there is constructive interference between the seismic events representing the top and base of the 6 m thick steamed zone.

The logs plotted in Figures 2 and 3 were modified to simulate the other cases listed above. For case (b), a tight streak and a gas-saturated interval from 426 m to 436 m were inserted and the original gas interval deleted. Case (c), the cold reservoir model for the top of the Clearwater Formation, was created by deleting the gas interval. The 6 m steam zone of case (d) was extended to 18 m for case (e) and deleted for case (f). In each case the densities were modified accordingly.

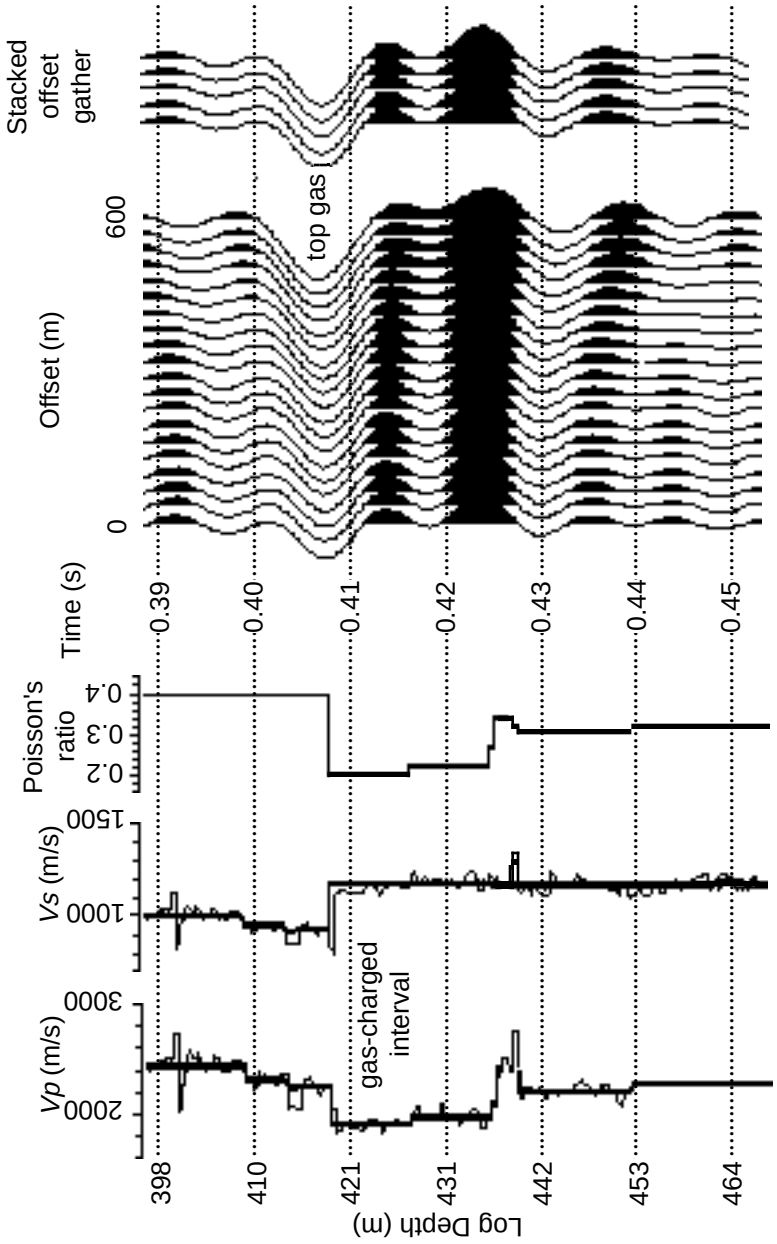

Fig. 2. Plots of the *P*-wave and *S*-wave sonic logs and calculated Poisson's ratios used to generate the synthetic seismic offset gather displayed. Offsets up to 600 m were included in the gather. These traces were stacked and repeated five times to produce the stacked gather. The model is for case (a): a gas-saturated interval at the top of the Clearwater Formation, from 418 m to 433 m depth.

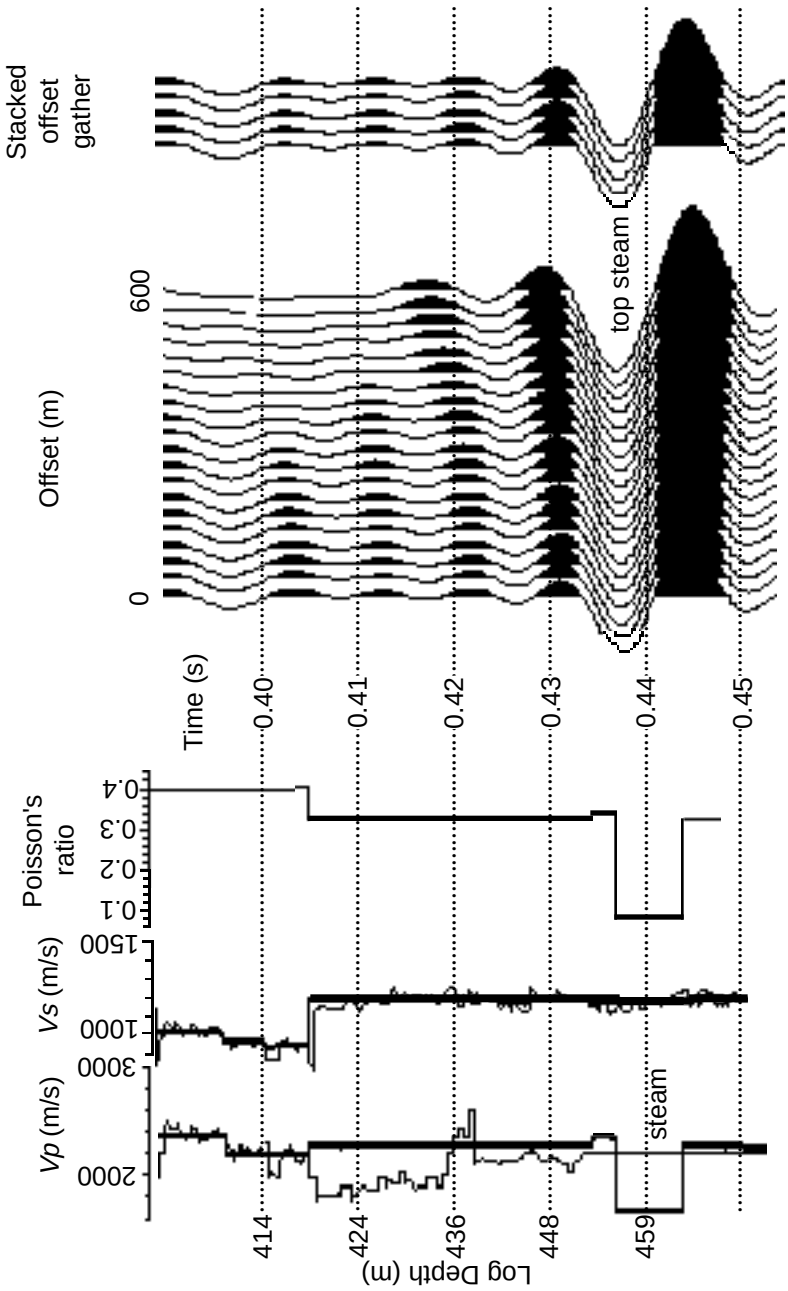

Fig. 3. Plots of the *P*-wave and *S*-wave sonic logs and calculated Poisson's ratios used to generate the synthetic seismic offset gather displayed. Offsets up to 600 m were included in the gather. These traces were stacked and repeated five times to produce the stacked gather. This model is for case (d): a steamed interval at the depth of the perforations, from 457 m to 463 m depth.

The synthetic seismic offset gathers generated for each of these six models are presented in Figures 4 and 5. Figure 4 shows the traces generated for the gas cases (a) and (b) and the gas-free case (c). The traces displayed in Figures 4a, 4c and 4e were generated using an Ormsby bandpass wavelet with frequency limits 10/15-100/120 Hz while the traces in Figures 4b, 4d and 4f were generated using extracted wavelet (1). Annotated are the top of the reservoir and the top of the gas zone.

For Figures 4a and 4b the gas zone is modelled at the top of the reservoir, as seen in Figure 2, and its top correlates to the trough at 0.407 s. The amplitude of this trough increases slightly with increasing offset. For Figures 4c and 4d the gas zone is modelled below a tight streak and its top correlates to the trough at 0.417 s, which corresponds to the time of some of the amplitude anomalies on the 1990 seismic data. It is hard to judge from this display the behaviour of the amplitudes as a function of offset. The presence of gas at a depth of 8 m below the top of the reservoir changes the character of events at the top of the reservoir at 0.407 s because of interference. This can be seen by comparing the top reservoir events in Figures 4a and 4b with those in Figures 4c and 4d. It is especially noticeable in the traces generated using the extracted wavelet. In Figures 4e and 4f the top of the cold reservoir is at 0.407 s and appears as a weak event, which in Figure 4f changes phase with offset. In the absence of a heated zone at the top of the reservoir, the event corresponding to this top is difficult to pick on the seismic data. The stacked offset traces seen in Figure 3 show this event to be a weak trough at 0.407 s.

Similar offset gathers for the steamed zone cases are shown in Figure 5. In each case the depth of the top of the perforated zone correlates to a trough at 0.438 s, which is the time at which strong amplitude anomalies were observed on some of the 1992 seismic data. When the steamed interval is only 6 m thick (Figures 5a and 5b), constructive interference occurs between the events representing the top and base of the interval. Increasing the interval to 18 m causes the top and base to be resolved. The four gas cases in Figure 4 all exhibit an increase in amplitude with offset whereas if no gas is present, the event changes phase. In all four steam examples in Figure 5, the amplitude of the trough at 0.438 s is high at zero-offset and increases slightly with offset. When no steam is present, a trough is still observed but its zero-offset amplitude is, as expected, lower and its amplitude decreases with increasing offset.

Discrimination between an anomaly caused by partial gas-saturation and one due to steam does not appear to be possible. The presence of both fluids in a restricted interval within the reservoir results in a high amplitude trough (negative reflection coefficient). However, the conditions of high temperature and high fluid pressure in 1992 (steaming cycle) do not allow for the presence of gas, except in very thin layers (Eastwood et al., 1994). In 1990, the temperature and fluid pressure are lower and gas comes out of solution. It is assumed, therefore, that only steam anomalies are seen in the 1992 3-D data and only gas anomalies in the 1990 3-D data. At the AABBW pads, the situation is different. Fluid pressures during the steam injection cycle (1993) were lower than during steaming at the D3 pad (4-6.5 MPa compared to 8-10 MPa) so gas is present during the steaming cycle (J. Eastwood, *pers. comm.*). Thus, in the 1993 3-C data, anomalies may be caused by both gas and steam. Gas anomalies may be expected at the top of the reservoir, as in 1990 3-D data, while steam anomalies may be seen at the perforation depth, as in the 1992 3-D data.

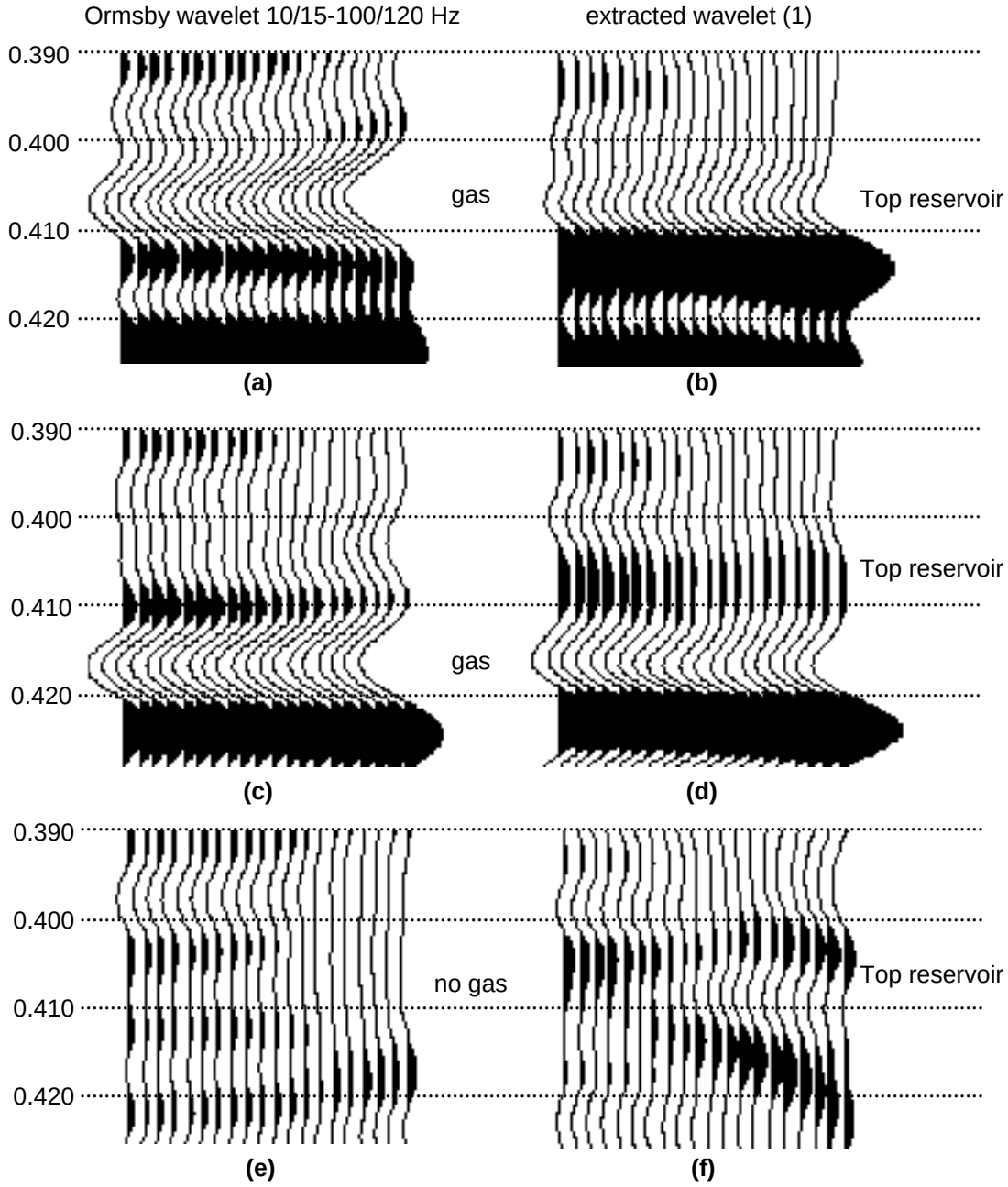

Fig. 4. Synthetic offset gathers generated from gas models. Plots **(a)**, **(c)** and **(e)** were generated using an Ormsby bandpass wavelet while plots **(b)**, **(d)** and **(f)** were generated using extracted wavelet (1). Plots (a) and (b) show the modelled results of a gas-saturated interval at the top of the reservoir; (c) and (d) for a gas-saturated zone 8 m below the top of the reservoir, beneath a tight streak; (e) and (f) for the cold reservoir top.

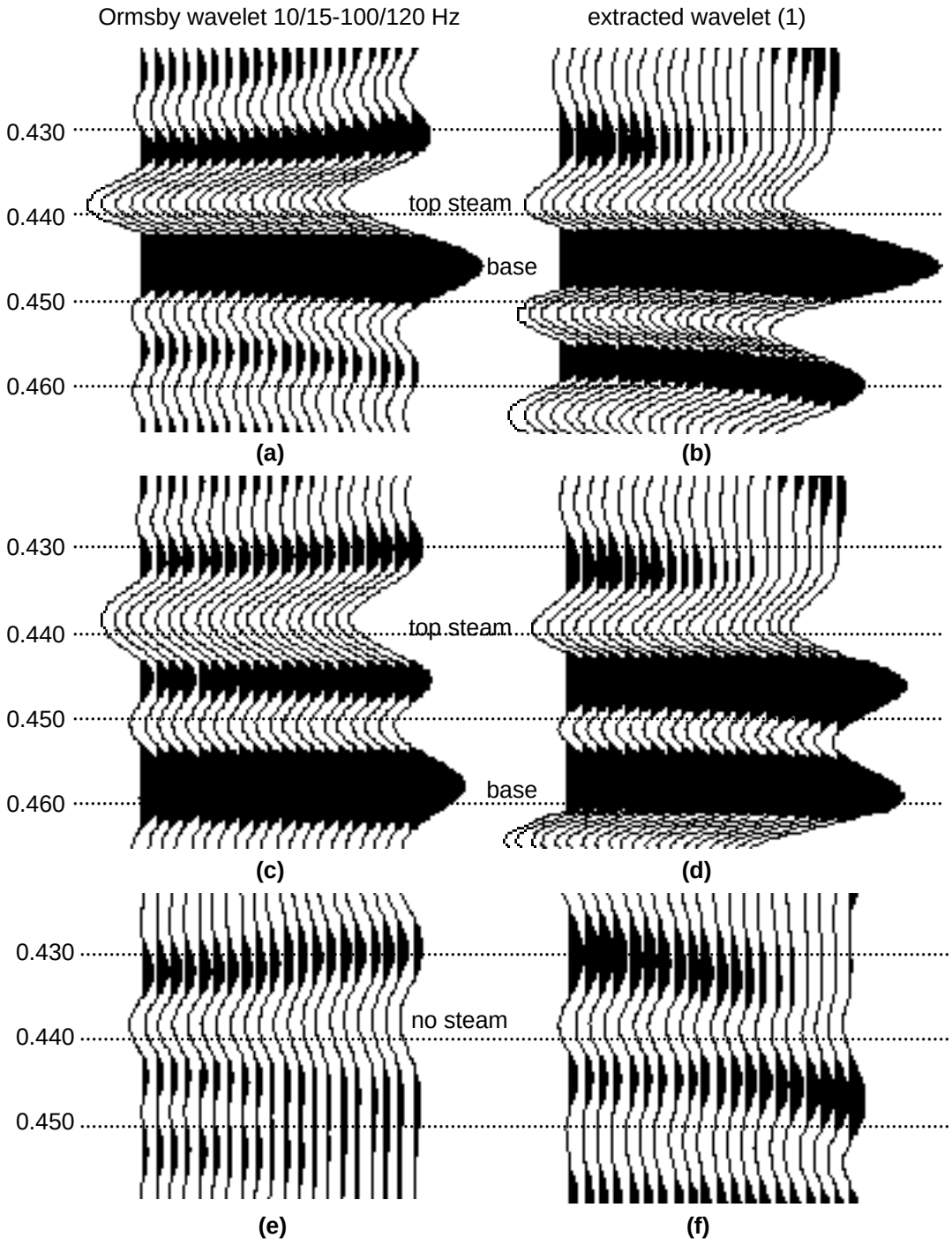

Fig. 5. Synthetic offset gathers generated from steam. Plots **(a)**, **(c)** and **(e)** were generated using an Ormsby bandpass wavelet while plots **(b)**, **(d)** and **(f)** were generated using extracted wavelet (1). Plots (a) and (b) show the modelled results of a 6 m steam-saturated interval at the perforation depth; (c) and (d) for an 18 m steam-saturated interval; (e) and (f) for the cold reservoir at the perforation depth.

Examples of amplitude anomalies observed on the seismic data and their correlation to the synthetic stacked traces are shown in Figures 6 and 7. The synthetic traces in these figures were generated using extracted wavelet (1).

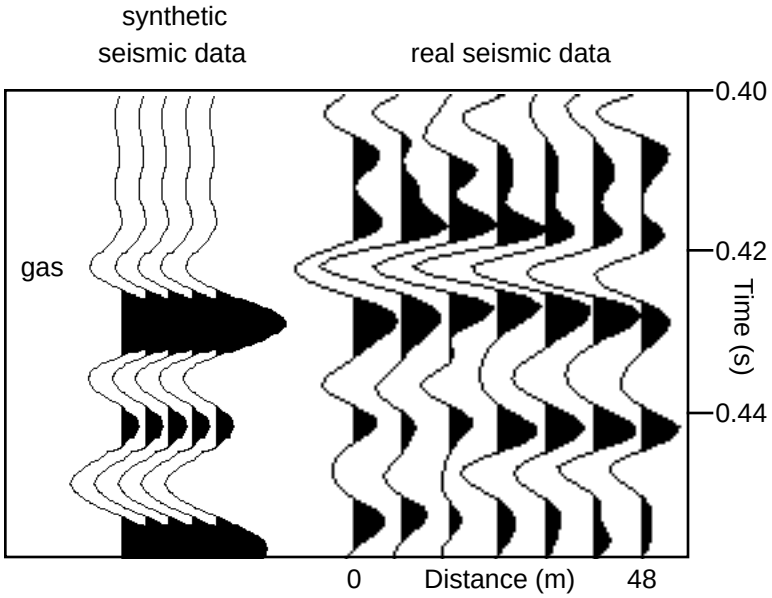

Fig. 6. An interpreted gas anomaly in the 1990 stacked data and the synthetic stacked section created from the model with gas below a tight streak (case b). The synthetic data were generated using extracted wavelet (1).

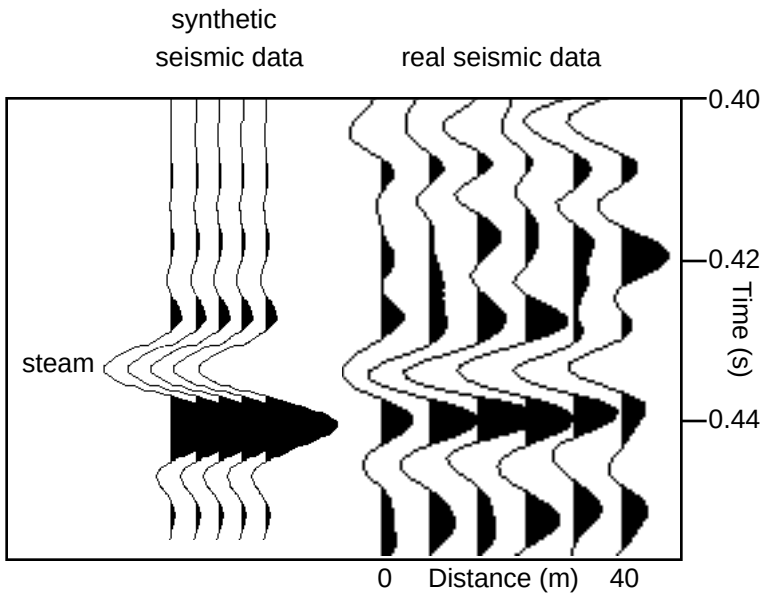

Fig. 7. An interpreted steam anomaly in the 1992 data and the synthetic stacked section created from a model with a 6 m steamed zone at the perforation depth (case d). The synthetic data were generated using extracted wavelet (1).

In Figure 6 the amplitude anomaly on the 1990 stacked data is interpreted to be caused by partial gas-saturation below a tight streak and the synthetic traces were created from the model of such an interval (case b). The amplitude anomaly at 0.437 s in Figure 7 is interpreted to be due to a steamed zone at the depth of the perforations. The traces were generated using the model in Figure 3 (case d). The match between the synthetic traces and the real seismic data is very good and confirms that the models are realistic.

The McMurray/Devonian interface was also modelled by appending a section to each log (Figure 8). A constant velocity was used within each unit, taken from sonic log and stacking velocities and theoretical *Vp/Vs* values. This interface was modelled to observe the behaviour of the top Devonian amplitudes and to ensure that the event exhibited no anomalous amplitude changes over the range of offsets to be used in the analysis. The Devonian event is seen to be a high amplitude peak just below 0.5 s, whose amplitude increases significantly only at the farthest offsets. It will be shown that the farthest offsets must be limited to 500 m because of this increase in amplitude.

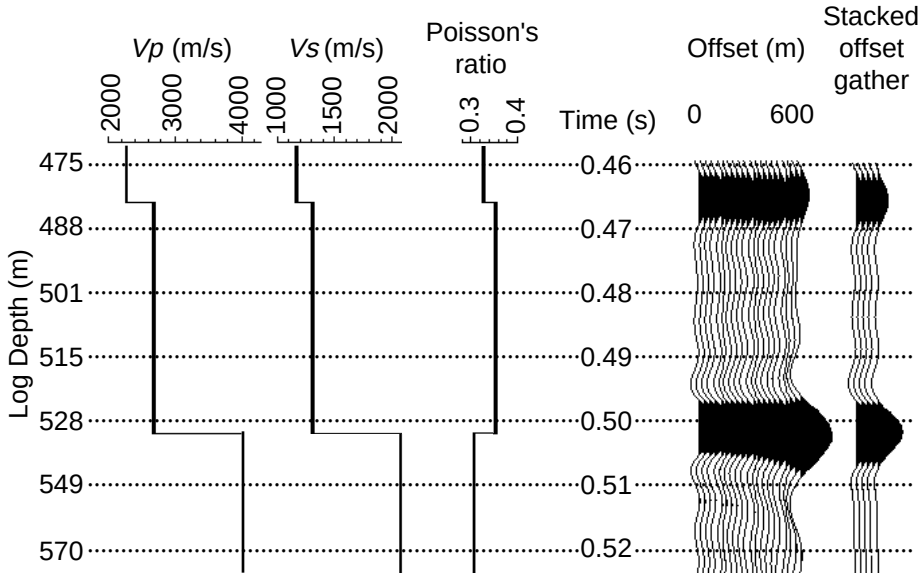

Fig. 8. Model for the McMurray/Devonian interface, which occurs at 530 m.

Amplitude extraction

To observe in more detail the behaviour of the modelled seismic amplitudes with offset, amplitudes were extracted from the twelve seismic gathers displayed in Figures 4 and 5. Since the wavelet used in the generation of the seismic data is not a simple spike and individual boundaries on well logs are closely spaced, the seismic response to a boundary is not a single, unique event but a combination of interfering events. To obtain meaningful amplitudes, therefore, rms amplitudes were extracted over 10 ms time windows centred on the events under investigation.

Figures 9a and 9b show the signed rms amplitudes for gas at the top of the reservoir, gas below a tight streak and no gas. Figures 9c and 9d display signed rms amplitudes for a 6 m steam zone, an 18 m steam zone and no steam. Since the cold reservoir amplitudes are very low, they are shown on each plot in an insert, at a greatly enlarged vertical scale, so their behaviour with offset can be observed.

The amplitude scales on Figures 9a and 9c are comparable, as are those on Figures 9b and 9d. The amplitude extraction window was centred on 0.408 s for the top reservoir models (gas and cold) and at 0.417 s for the gas below the tight streak.

When an Ormsby bandpass wavelet is used in the generation of the synthetic seismic data (Figure 9a), both cases of gas in the reservoir result in an increase in absolute amplitude with increasing offset (up to 500 m), although the increase is more pronounced when gas is at the very top of the reservoir. When there is no gas present, the absolute amplitudes decrease gently but the effect may be too small to be observed on field data. For the extracted wavelet (1) data (Figure 9b), the amplitude behaviour is more complicated. Gas at the top of the reservoir still results in a significant increase in absolute amplitude with offset but when gas is present below a tight streak, the absolute amplitudes increase to an offset of about 250 m then decrease to 440 m before increasing again. The overall effect over the range of 600 m is almost no AVO gradient. If the farthest offset in real data lies between 300 m and 500 m, a negative gradient may be seen. When no gas is present in the reservoir, the absolute amplitudes decrease to 250 m then increase; the overall effect is a slight increase of amplitude with offset.

Modelling of the steamed zone produces clearer results, as they are similar for both the bandpass and extracted wavelet (1) data. These results are presented in Figures 9c and 9d (Ormsby bandpass wavelet data and extracted wavelet (1) data, respectively). The amplitude extraction window was centred on 0.438 s. The zero-offset amplitude of the 6 m steamed zone is higher than that of the 18 m steamed zone, because of tuning effects in both cases. The absolute amplitudes increase with increasing offset, especially at the farther offsets. The cold perforation zone sees a decrease in absolute amplitude for both wavelets, although in both cases the zero-offset reflectivity is low and the decrease in amplitude is small.

The results of this modelling indicate that a measurable increase in rms amplitude with increasing source-receiver offset should be observed on processed field seismic data when steam is present within the reservoir. When gas is present in the reservoir, an increase should also be seen but may not be apparent if the gas is trapped below a tight streak. If no gas is present, a low zero-offset reflectivity value is observed but the overall amplitude behaviour depends on the convolving wavelet. Data containing a complex extracted wavelet may produce ambiguous results if all offsets up to 600 m are used in the AVO analysis. For the cases of no gas and gas at the top of the reservoir, an increase in amplitude with offset is the overall effect over the full 600 m offset range. If the offsets are restricted to about 250 m, then the no-gas case should produce an amplitude decrease with offset whereas the gas case should show an increase. When gas is present below a tight streak, a positive, flat or negative gradient may be seen depending on the farthest offset present in the gathers. If the offsets are limited to less than 250 m, an increase in amplitude should be seen. Thus, for the processed field seismic data, if offsets are restricted to less than 250 m, the two gas cases should produce an increase in amplitude with increasing offset, whereas the no-gas case should produce a decrease.

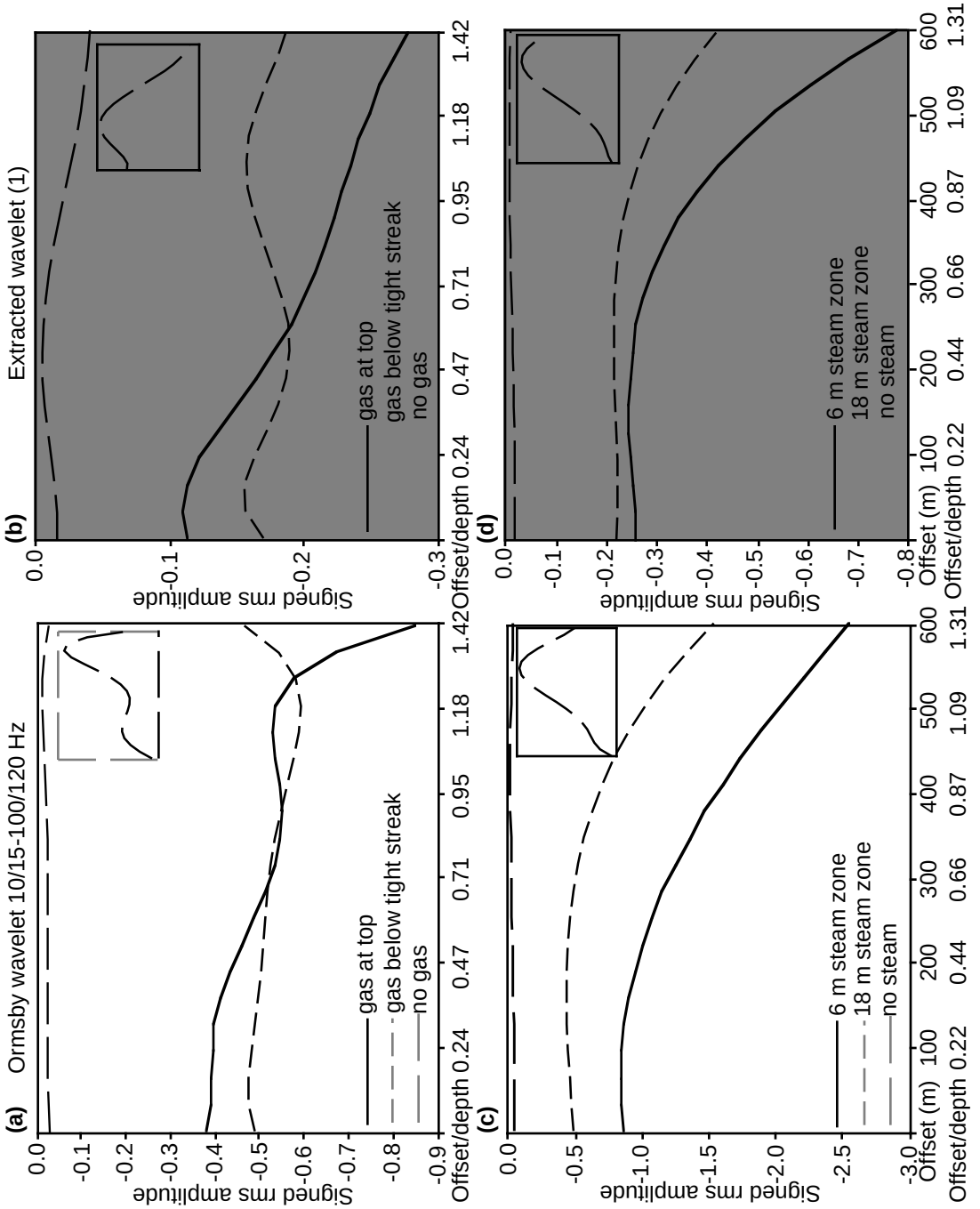

Fig. 9. Modelled amplitudes extracted from the synthetic seismic gathers over 10 ms windows. Plots **(a)** and **(b)** show amplitudes for the cases of gas at the top of the reservoir, gas below a tight streak and no gas. Plots **(c)** and **(d)** show amplitudes for the cases of a 6 m steam zone, an 18 m steam zone and no steam. The amplitudes shown in (a) and (c) are extracted from the data generated using an Ormsby wavelet while those in (b) and (d) are extracted from the data generated using extracted wavelet (1).

In a similar manner, rms amplitudes were extracted for the Devonian event to observe their behaviour, as this event was chosen to be the reference event for the Chiburis AVO analysis. These amplitudes are plotted in Figure 10, where it is seen that the amplitudes are reasonably consistent up to an offset of 500 m, particularly for the case using extracted wavelet (1). Beyond 500 m the amplitudes increase substantially, thus indicating that offsets over 500 m should probably not be used in the AVO analysis. This problem is addressed in the following discussion.

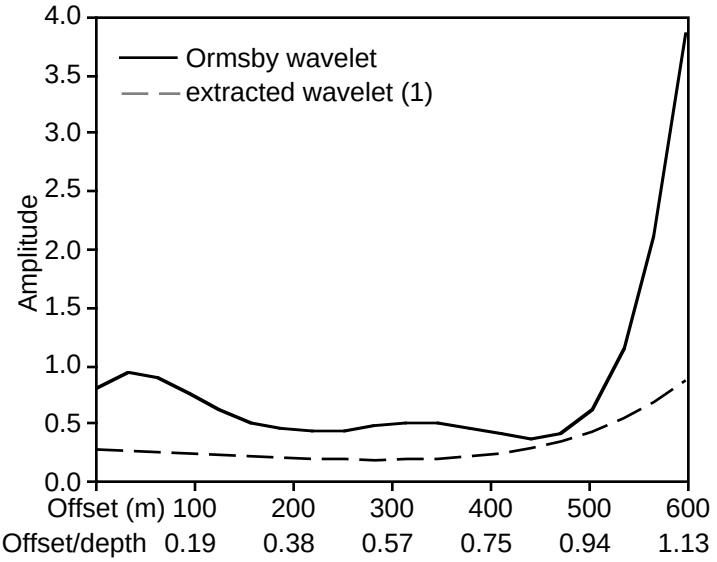

Fig. 10. Modelled rms amplitudes for the Devonian (reference) event.

Since the Chiburis method is the chosen method of AVO analysis for these data, the modelled extracted amplitudes were used to generate conditioned amplitude ratios. These ratios were calculated using equations 1 and 2, based on the rms amplitudes displayed in Figures 9 and 10, and the results are presented in Figure 11 for the gas cases and Figure 12 for the steam cases, for both the Ormsby bandpass wavelet and extracted wavelet (1).

The top plots in each figure show the calculated amplitude ratios for all offsets up to 600 m whereas in the lower plots the offsets are restricted to those less than 500 m. It is apparent that using offsets up to 600 m is likely to give ambiguous results. Restricting the offsets to 500 m results in amplitude ratio increases with offset for the gas cases modelled using an Ormsby bandpass wavelet. For the extracted wavelet (1), offsets must be restricted to those below about 250 m (offset squared = 0.625×10^5 m) if a distinction is to made between the gas cases and the no-gas case. The modelled amplitude ratios for the steam cases have an increase with offset for both the Ormsby wavelet and extracted wavelet (1) while for the non-steam case the ratios decrease with offset, for offsets up to 500 m.

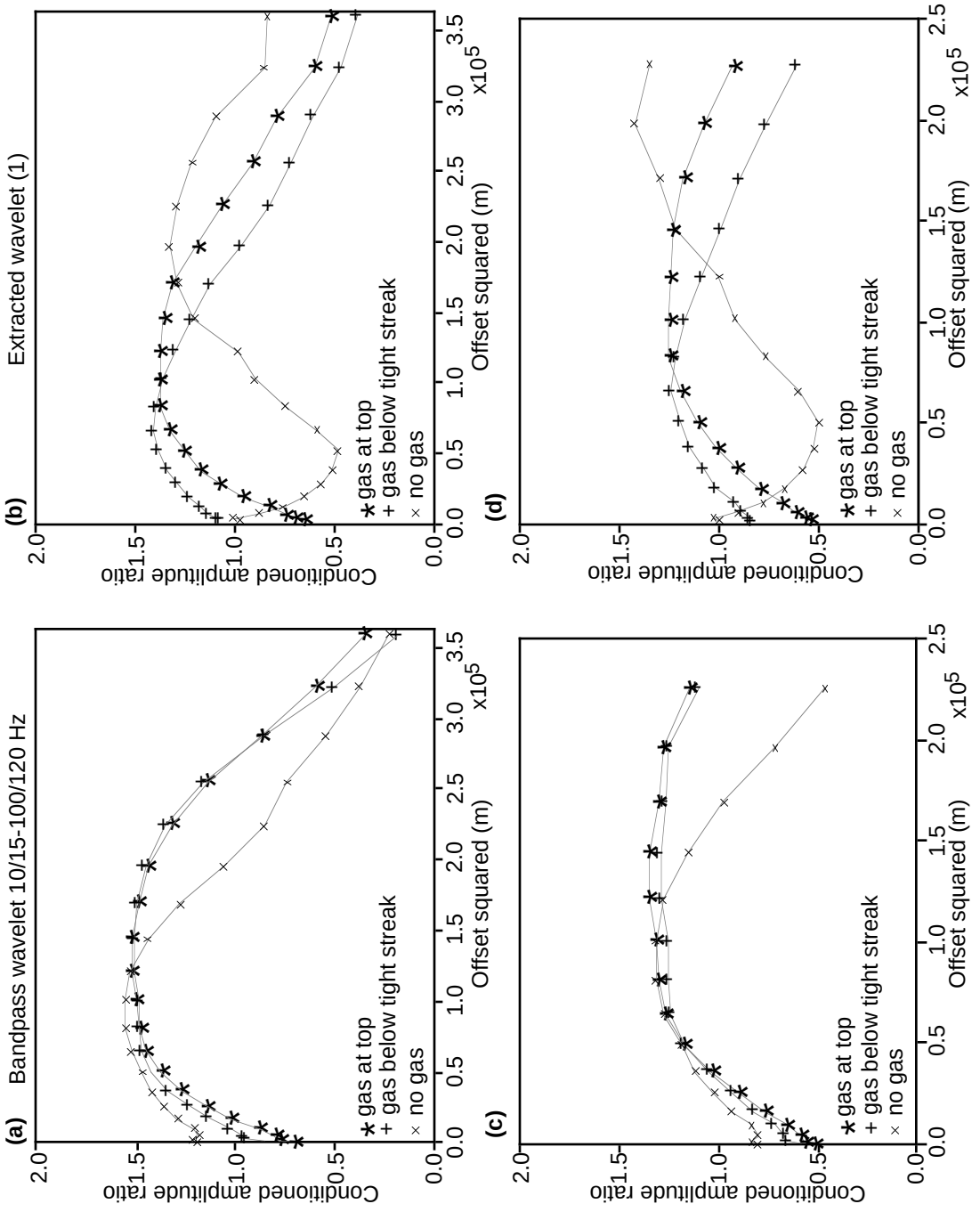

Fig. 11. Modelled conditioned amplitude ratios for the gas cases. In plots **(a)** and **(b)** offsets up to 600 m are included whereas in plots **(c)** and **(d)** offsets are restricted to less than 500 m. Extracted wavelet (1) is that one derived from the 1990 3-D seismic data.

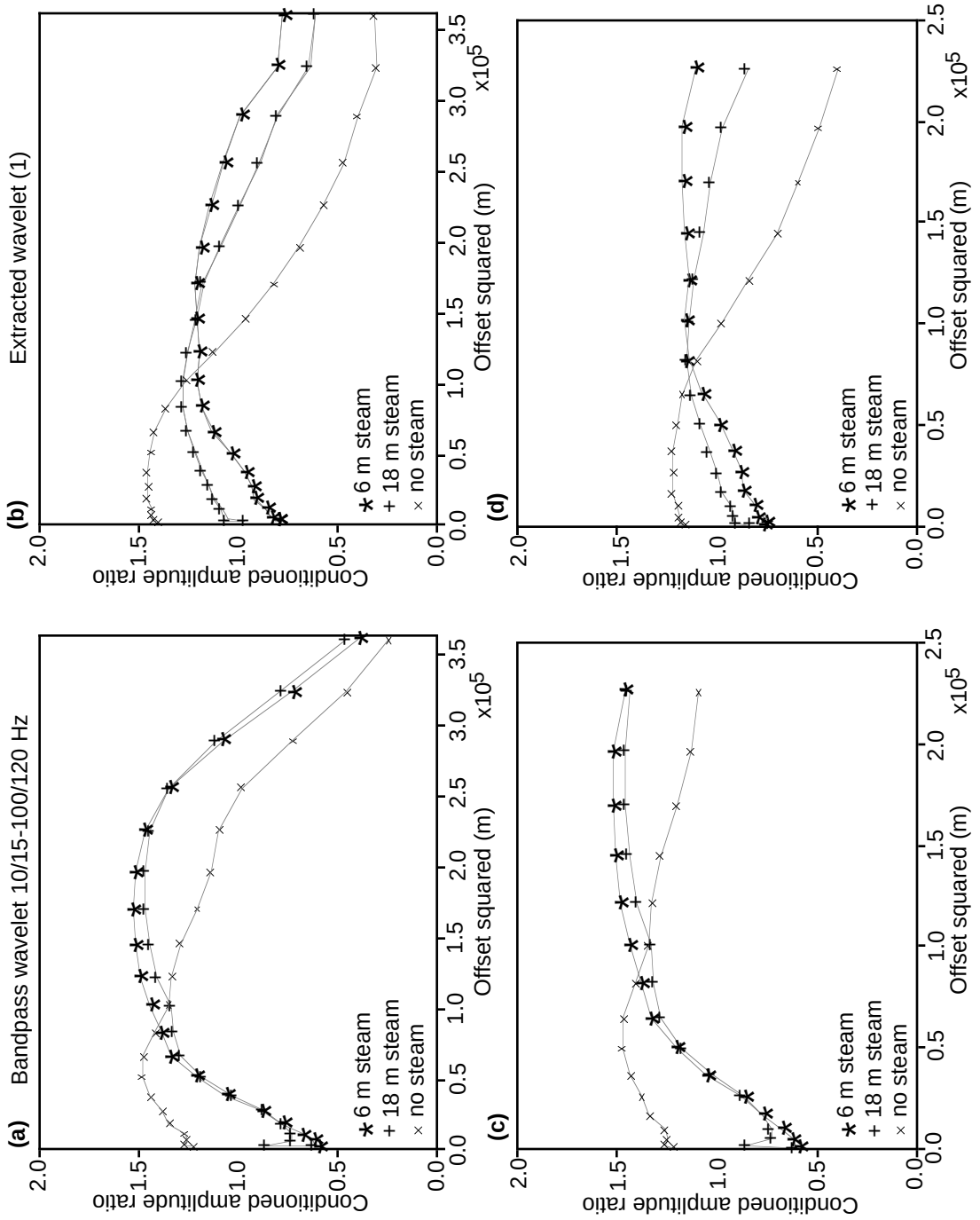

Fig. 12. Modelled conditioned amplitude ratios for the steam cases. In plots **(a)** and **(b)** offsets up to 600 m are included whereas in plots **(c)** and **(d)** offsets are restricted to less than 500 m. Extracted wavelet (1) is that one derived from the 1990 3-D seismic data.

Similar synthetic seismic gathers were also generated using extracted wavelet (2), which was derived from the 3-C data. Modelled cases were those of gas at the top of the reservoir and no-gas. The Chiburis conditioned amplitudes extracted from these gathers are plotted in Figure 13 and indicate that all offsets (up to 500 m) should be used in the analysis of gathers created from these 3-C data. For the 3-D data gas cases (Figure 11), it was clear that offsets had to be restricted to under 250 m to avoid ambiguity.

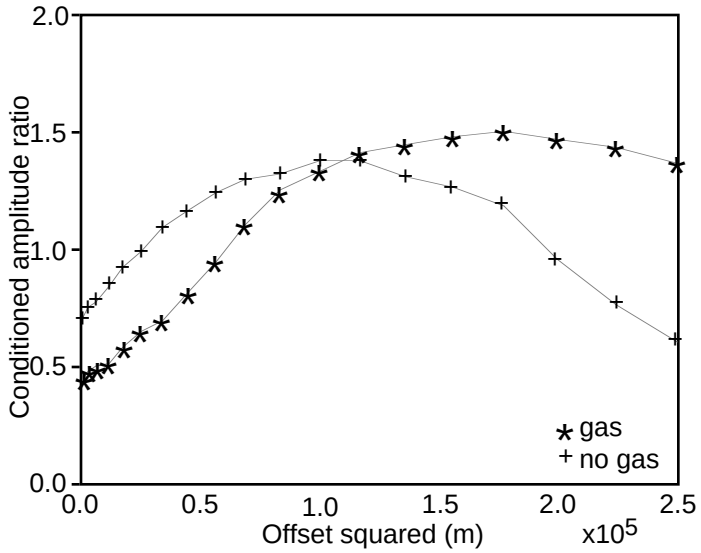

Fig. 13. Modelled conditioned amplitude ratios from synthetic seismic data created with extracted wavelet (2), from the 3-C data.

AVO ANALYSIS OF PRE-STACK SEISMIC DATA

The seismic data used in the AVO analysis were the *P-P* data from line 470-93 at the AABBW pads and the two 3-D surveys at the D3 pad. Careful, amplitude-preserving and surface-consistent processing (including static corrections, deconvolution and amplitude balancing) is recommended for data to be used in AVO analysis (Yu, 1985; Allen and Peddy, 1993). Each data set from Cold Lake had spherical divergence compensation applied then trace amplitude balancing designed over a window the length of the whole trace, in order to retain relative amplitude information. Surface-consistent deconvolution was applied to the 3-D data volumes whereas record-based spiking deconvolution and surface-consistent refraction static corrections were applied to line 470-93. The data were also NMO-corrected and NMO stretch was muted.

Pre-stack migration is recommended to collapse the Fresnel zone and correctly position events (Allen and Peddy, 1993; Jones et al., 1995). For the 3-D seismic data, up to 150 CDP gathers were extracted from the data volume around several areas of interest. These gathers and all the CDP gathers along line 470-93 were pre-stack time-migrated using *f-k* migration. Each NMO-corrected, muted gather was restricted to offsets less than 500 m. The individual data sets were sorted into common offset gathers and pre-stack *f-k* migrated in that domain before being resorted into CDP

gathers. Finally the data were bandpass filtered between frequency limits of 10/15-100/120 Hz.

3-D data selection

Anomalies for AVO analysis were chosen from amplitude maps of the migrated 3-D data and of the "difference" 3-D data set, created by subtracting the 1990 data from the 1992 data. Anomalies were analysed over a 10 ms time window centred on 0.42 s for the 1990 data and on 0.437 s for the 1992 data and over corresponding windows for the difference data. The two difference data amplitude maps will be referred as "shallow" and "deep", for clarity. It is interpreted that anomalies on the 1990 amplitude map are caused by gas-saturated zones and, possibly tight streaks, because the spatial distribution of anomalies on the stacked data and shallow difference data amplitude maps are not always the same. Tight streaks should not appear on the shallow difference amplitude map because they are present in both the 1990 and 1992 data. If the low velocity interval is present in only one vintage of data (1990 or 1992), anomalies should appear on both the time data amplitude map for that vintage of data, and on the difference data amplitude map. On the 1992 amplitude map, the anomalies are interpreted to be caused mainly by the presence of steam with few tight streaks, because the spatial distribution of anomalies on the stacked data and deep difference data amplitude maps are similar.

Six areas for analysis of the 1990 data were selected on the basis that amplitude anomalies appeared on both amplitude maps (1990 stacked data and shallow difference data), on only one map or on neither. Similarly, six areas were chosen from the 1992 stacked data amplitude map and the deep difference amplitude map. These six areas are indicated in Figure 14, which shows the 1990 stacked amplitude and shallow difference amplitude maps, and Figure 15, which shows the 1992 stacked amplitude and deep difference amplitude maps. In the 1990 data, most of the amplitude anomalies are observed at about 0.420 s while in the 1992 data most of the anomalies are deeper, near 0.437 s. The areas selected for analysis are listed in Tables 1 and 2. In the comments column of each of these tables are given the interpretations of the anomalies. The anomalies are attributed to gas if seen in the 1990 data (areas 3, 4, 5, 6 and 7) and steam if seen in the 1992 data (areas 1, 4, 8, 10, 11 and 12). One area from each survey (2 and 9) was chosen because anomalies appeared on none of the amplitude maps.

Examples of some of the analysed anomalies are displayed in Figures 16 and 17, where corresponding extracts of stacked, migrated seismic data from the 1990 and 1992 surveys are shown. On the coloured version of these plots, reds represent negative reflection coefficients (troughs) and blues represent positive reflection coefficients (peaks). The analysed anomalies are indicated by arrows.

Figure 16 shows anomalies near 0.420 s that were selected from the 1990 amplitude map and shallow difference map in Figure 14. Figures 16a and 16b show an anomaly which is present on the 1990 data but not on the 1992 data (anomaly 6). It is interpreted to be a gas anomaly. In Figures 16c, 16d, 16e and 16f, anomalies are present on both vintages of data, although appearing a little stronger on the 1990 lines. These anomalies are present on the 1990 time amplitude map but the difference in amplitude between the 1990 and 1992 lines is not large enough to generate a strong anomaly on the shallow difference amplitude map. In Figures 16c and 16d the anomaly (number 4) appears as a trough below a peak, which could be a gas-saturated zone beneath a tight streak in 1990 and steam below the tight streak in 1992.

Table 1. Analysed amplitude anomalies from the 1990 stacked data and shallow difference data maps in Figure 14.

Area	Location	1990 amplitude anomaly	Difference amplitude anomaly	Comments
1	iline 23 xline 27	no	yes	Anomaly only in 1992. Interpreted steam in 1992.
2	iline 29 xline 52	no	no	No anomaly on either.
3	iline 30 xline 65	yes	yes	Anomaly only in 1990. Interpreted gas in 1990.
4	iline 31 xline 11	yes	no	Interpreted gas in 1990 and steam in 1992.
5	iline 41 xline 60	yes	no	Probably gas in 1990 but tight streak likely in 1992.
6	iline 50 xline 48	yes	yes	Anomaly only in 1990. Interpreted gas in 1990.

Table 2. Analysed amplitude anomalies from the 1992 stacked data and deep difference data maps in Figure 15.

Area	Location	1992 amplitude anomaly	Difference amplitude anomaly	Comments
7	iline 21 xline 64	no	yes	Anomaly in 1990 (possibly gas). No steam in 1992.
8	iline 23 xline 19	yes	no	Anomaly on 1992 and 1990. Interpreted as steam in 1992 and gas in 1990.
9	iline 29 xline 42	no	no	Anomaly on neither.
10	iline 37 xline 16	yes	yes	Anomaly only in 1992 data. Interpreted steam in 1992.
11	iline 37 xline 52	yes	yes	Anomaly only in 1992 data. Interpreted steam in 1992.
12	iline 46 xline 17	yes	yes	Anomaly only in 1992 data. Interpreted steam in 1992.

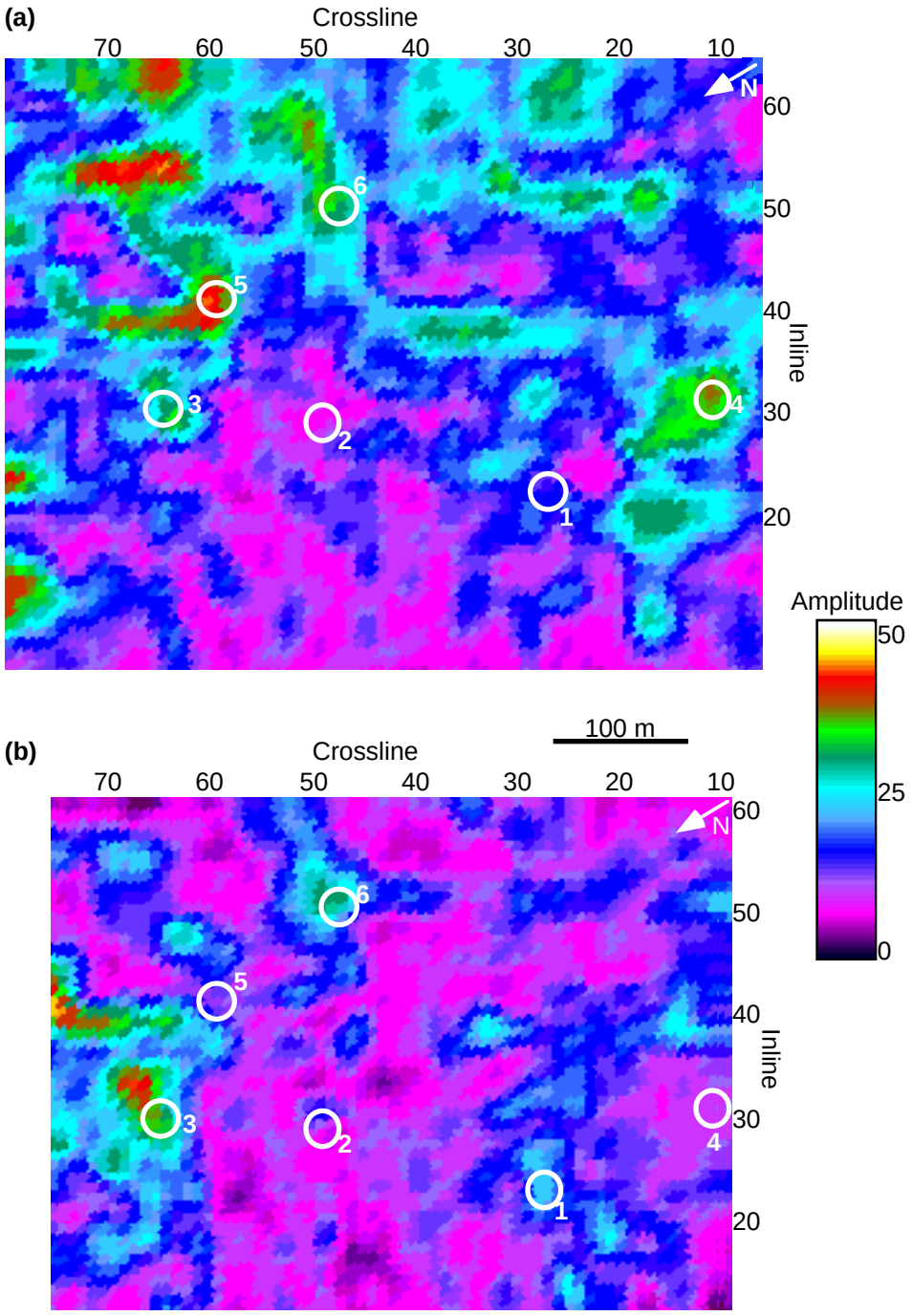

Fig. 14. Analysed anomalies from the **(a)** 1990 time amplitude map and **(b)** shallow difference amplitude map, over a 10 ms window centred on a time of 0.42 s.

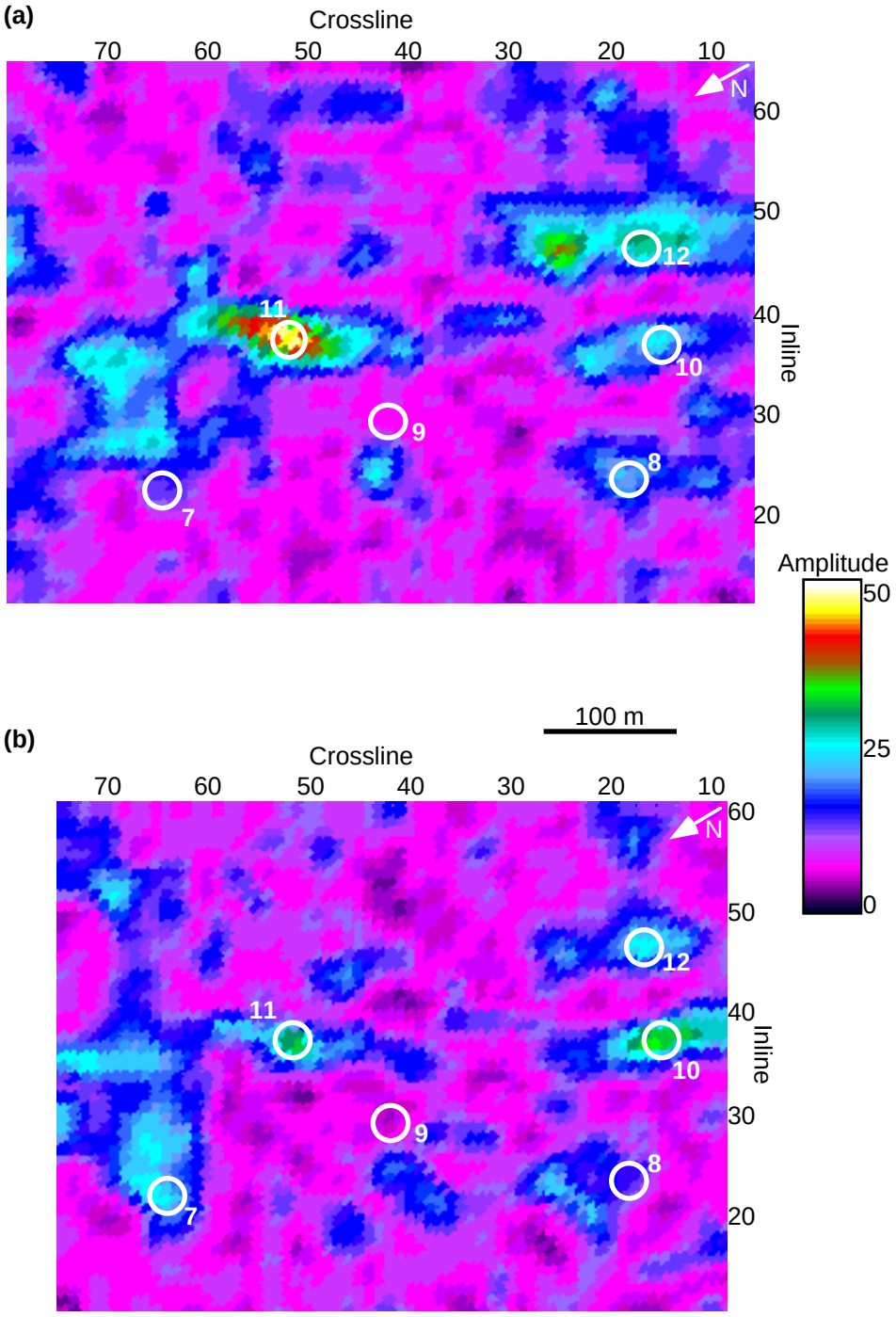

Fig. 15. Analysed anomalies from the **(a)** 1992 time amplitude map and **(b)** deep difference amplitude map, over a 10 ms window centred on a time of 0.437 s.

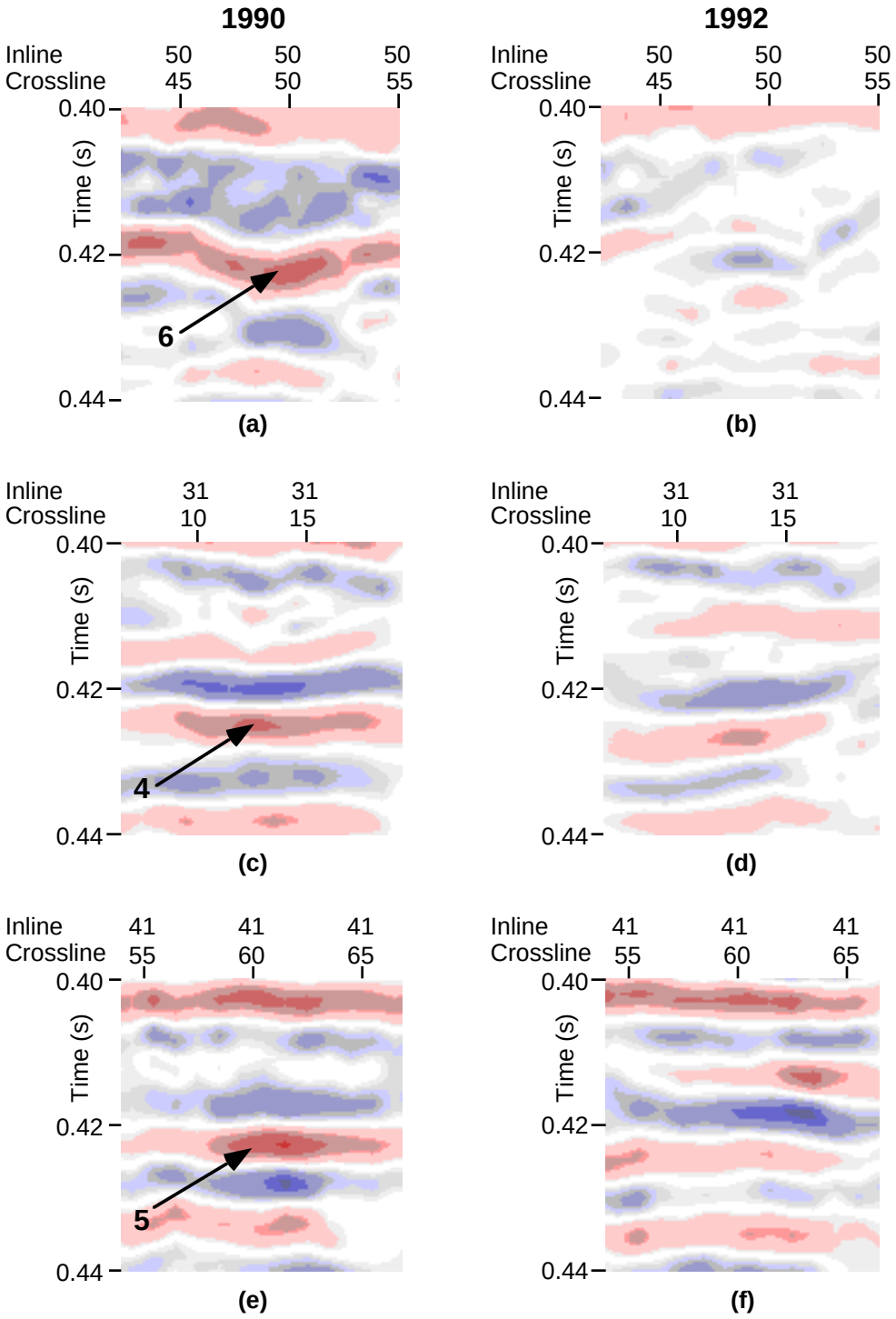

Fig. 16. Examples (numbered) of amplitude anomalies selected from the 1990 amplitude and shallow difference amplitude maps. Anomalies occur near 0.420 s.

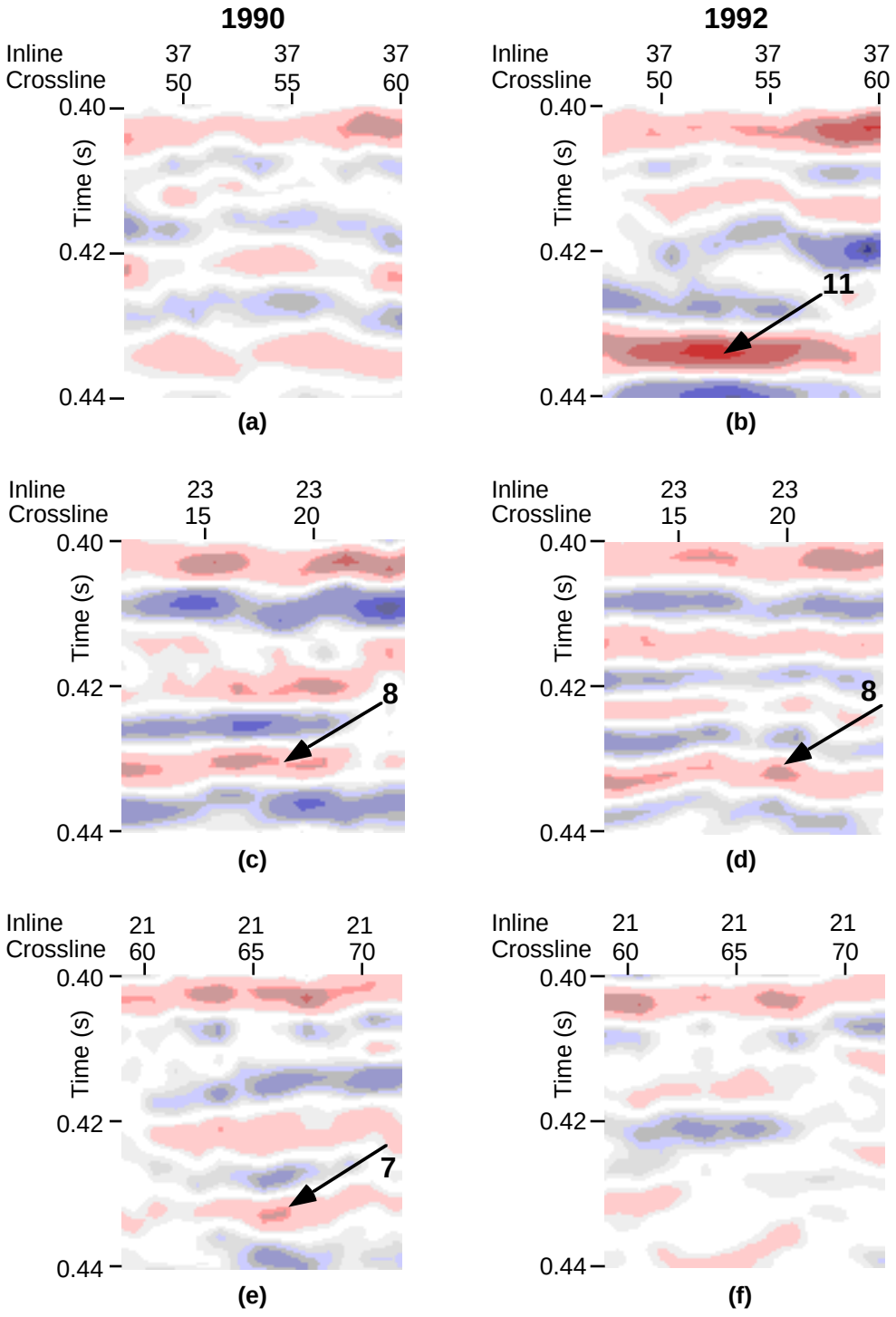

Fig. 17. Examples (numbered) of amplitude anomalies selected from the 1992 amplitude and deep difference amplitude maps. Anomalies occur near 0.437 s.

In Figures 16e and 16f (anomaly 5) there is a high amplitude trough on the 1990 data at 0.425 s but on the 1992 data the overlying peak has the higher amplitude. It appears that gas may be present in 1990 but the 1992 situation is uncertain. It is possible that the amplitudes contributing to the anomaly in 1992 come from the peak above 0.42 s rather than the trough beneath, so steam may not be present in 1992.

Figure 17 shows anomalies near 0.437 s, selected from the 1992 amplitude map and the deep difference map in Figure 15. A very high amplitude anomaly on the 1992 line in Figure 17b is absent from the 1990 data in Figure 17a and is interpreted to be caused by the presence of steam (anomaly 11). Figures 17c and 17d show anomalies on both vintages of data (anomaly 8). Possibly steam was present in 1992 and gas in 1990, both trapped beneath a tight streak. The final example shows an amplitude anomaly on the 1990 data but not on the 1992 data (anomaly 7); selected as a no steam case. Gas could be present in 1990.

AVO analysis of 3-D data

Supergathers were created from adjacent CDP gathers along three inlines and three crosslines centred on each of the twelve selected anomalies. Examples of two of the analysed supergathers are presented in Figures 18 and 19.

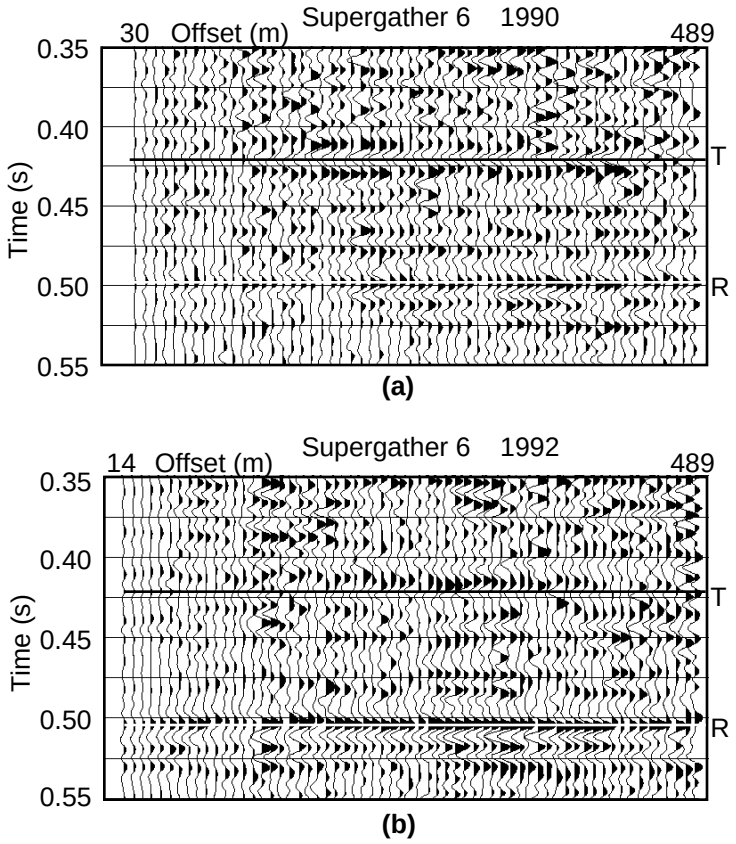

Fig. 18. Supergather 6, created to analyse an amplitude anomaly observed on the 1990 stacked data but not on the 1992 data. "T" denotes the target event and "R" the reference event (Devonian).

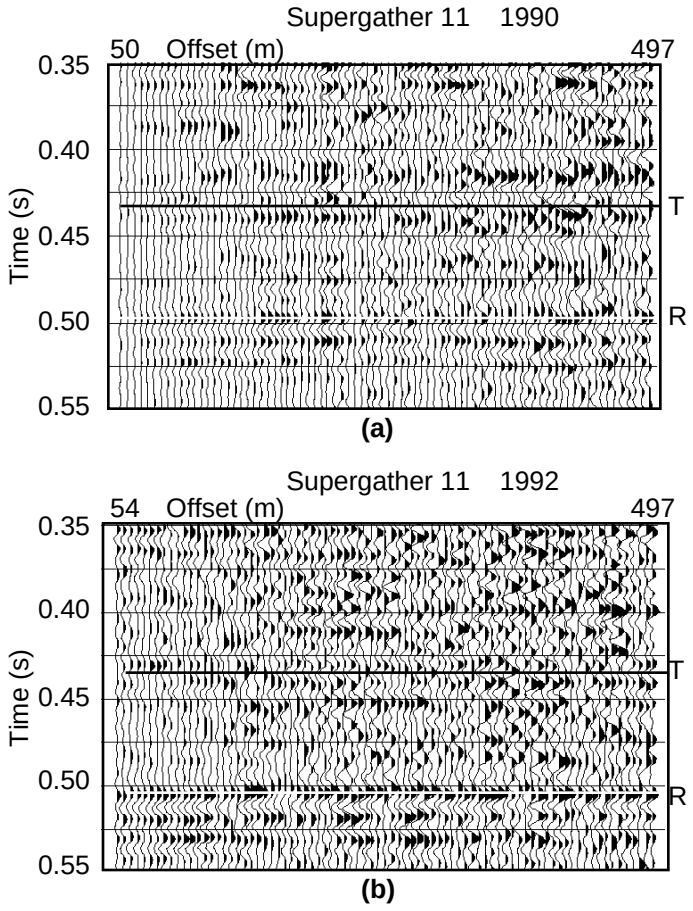

Fig. 19. Supergather 11, created to analyse an amplitude anomaly observed on the 1992 stacked data but not on the 1990 data. "T" denotes the target event and "R" the reference event (Devonian).

Supergathers (Ostrander, 1984) are designed to improve the signal to noise ratio of the data under analysis. These gathers were extracted from the pre-stack migrated, filtered data sets for both vintages of data. The traces in each supergather were sorted by offset then stacked into traces at offset spacings of 4 m, up to 500 m. Because of the geometry of the 3-D survey layout, not all offsets were present in the supergathers and those gathers nearer to the edges of the survey lacked the longer offsets. Each of the twelve anomalies was analysed on both the 1990 and 1992 data in order to provide two complementary assessments.

The apparently low zero-offset reflectivities seen on these gathers is caused by the filtering of shot-generated surface energy which was extremely strong at these near offsets. It is believed that relative amplitudes between the target and reference events are preserved. Figure 18 displays supergather 6, created to analyse an amplitude anomaly observed on the 1990 stacked data but not the 1992 data. This anomaly is interpreted to be caused by a gas-saturated zone in 1990. The target event (T) is at about 0.42 s and the reference event (R) is the Devonian horizon, which occurs a little later on the 1992 data than on the 1990 data. For the target event, a trough is seen clearly on the 1990 supergather while on the 1992 supergather the character of events at

this time of 0.42 changes with offset. The maximum amplitude of each trough or peak was picked interactively; the straight line annotated on the figures is meant only to indicate the approximate arrival time of the analysed events. Supergather 11 is shown in Figure 19. An amplitude anomaly which is observed on the 1992 stacked data at about 0.438 s, but is absent from the 1990 data, is interpreted to be caused by the presence of steam in 1992. The arrival time of the reference event is significantly later on the 1992 supergather. Target and reference events were picked interactively on each pair of twelve supergathers and the amplitudes of each event were extracted from the data over a 10 ms time window centred on the pick of that event.

Chiburis's method was used to calculate the conditioned amplitude ratio for each offset in the supergathers. An example of plots of raw amplitudes and conditioned amplitude ratios is presented in Figure 20. In this case, an increase in amplitude with offset is seen clearly on the raw amplitudes for the target event; this increase is retained in the plot of conditioned amplitude ratios.

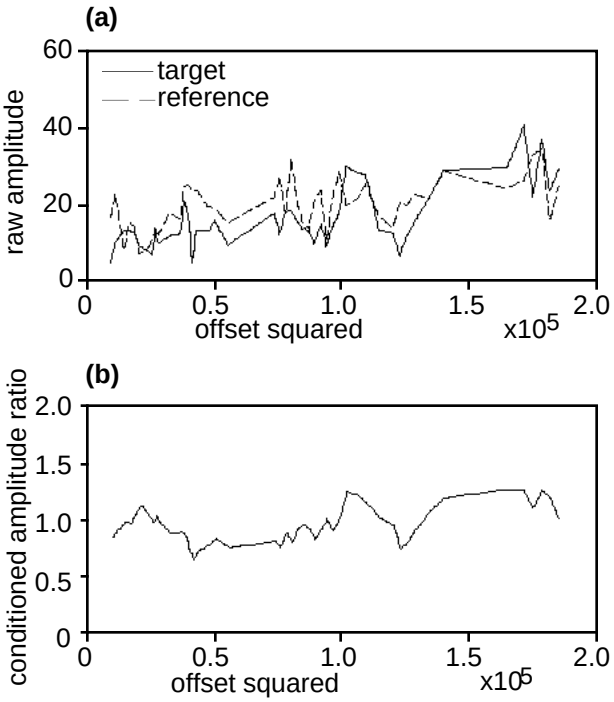

Fig. 20. Plot of the **(a)** raw amplitudes of the target and reference events and the **(b)** conditioned amplitude ratio. The increase in amplitude with offset observed in the raw amplitudes is preserved in the conditioned amplitude ratio.

Figure 21 shows these ratios for each of the supergathers 1 to 6, as determined from the 1990 data. Each star represents a conditioned amplitude ratio and the dashed line is a least-squares linear fit to these data points. It should be noted that the conditioned amplitudes are all scaled between 0 and 2 and do not represent the actual amplitudes of the target event. The magnitude of the zero-offset conditioned amplitude does not reflect the magnitude of the zero-offset reflectivity but the trend validly depicts the behaviour of amplitude with offset (Chiburis, 1984; 1993).

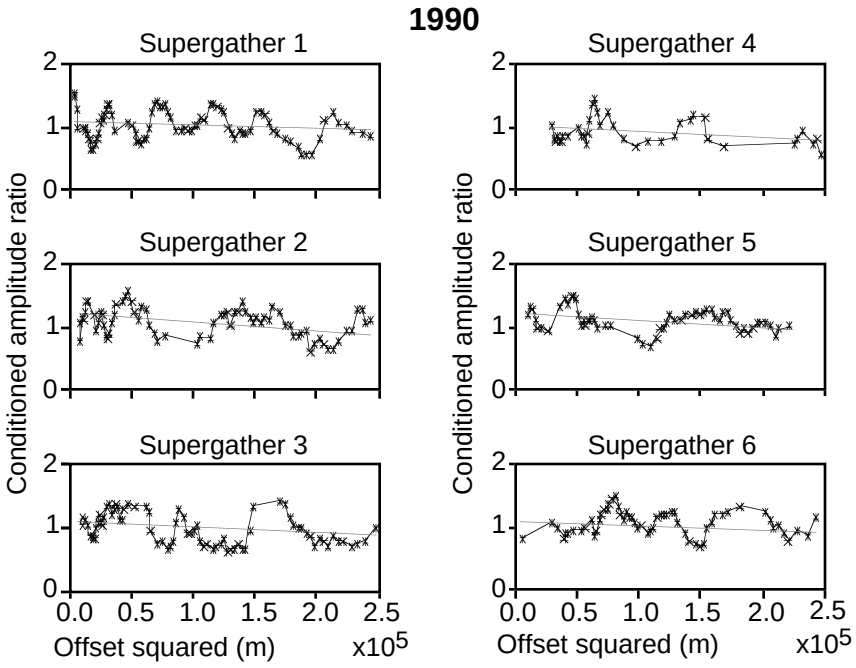

Fig. 21. Plots of conditioned amplitude ratio against offset squared (after Chiburis, 1984 and 1993) for supergathers 1 to 6, extracted from the 1990 data. All offsets up to 500 m are included.

For each supergather in Figure 21 a decrease in amplitude is observed with increasing offset, for offsets up to 500 m. The modelled amplitudes discussed in section 6.2.2 and presented in Figures 9 and 11 suggest that ambiguous results may be obtained over long offsets for the cases of gas below a tight streak and of no gas, which are the conditions under investigation with these 1990 supergathers. The plot in Figure 11d, which shows the modelled conditioned amplitude ratios calculated from a synthetic gather created with the extracted wavelet (1), suggests that limiting the offsets to those less than about 250 m would produce more definitive results. The gas case should show an increase in amplitude with offset while the no-gas case should show a decrease. Since the extracted wavelet (1) was obtained from these 1990 data under investigation, the offsets were limited to those less than 250 m and the analysis was repeated, with results shown in Figure 22. Now only supergather 1 has a decrease in amplitude with increasing offset. Supergathers 2, 3, 4, 5 and 6 show increases; those on supergathers 3 and 5 being large.

Corresponding conditioned amplitude ratios obtained from the AVO analysis of supergathers 1 to 6 from the 1992 data are plotted in Figure 23. Since steam, not gas, produces anomalies in the 1992 data, and there is no ambiguity in the modelled amplitudes for steam zones plotted in figures 12c and 12d, all offsets up to 500 m are included in the AVO analysis. Increases of amplitude with offset are seen clearly in Figure 23 for supergathers 1 and 4. On all of the other supergathers the trends are almost flat, although for supergathers 2 and 5 the gradients are negative, while for supergathers 3 and 6 they are positive.

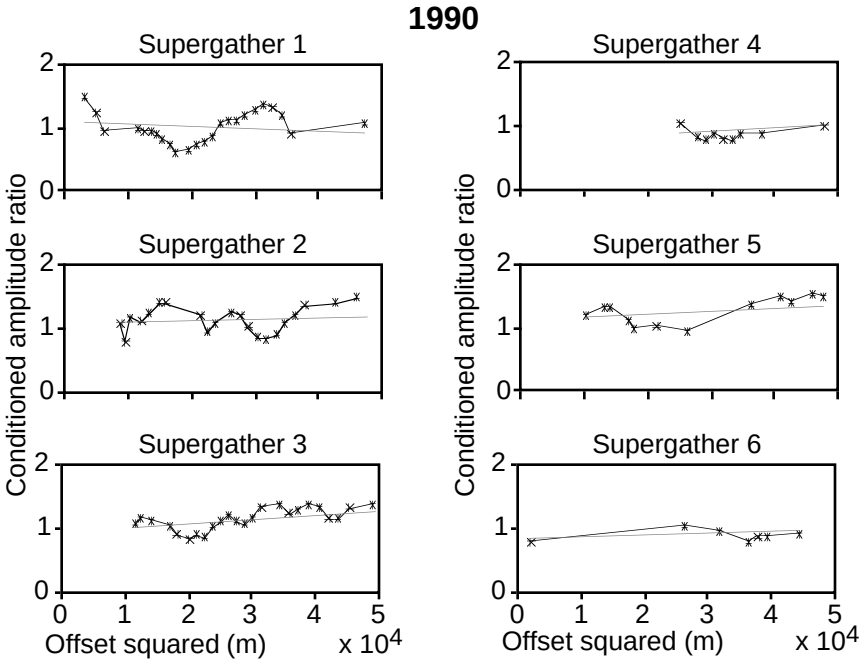

Fig. 22. Plots of conditioned amplitude ratio against offset squared for supergathers 1 to 6, extracted from the 1990 data. Offsets are limited to those below 250 m.

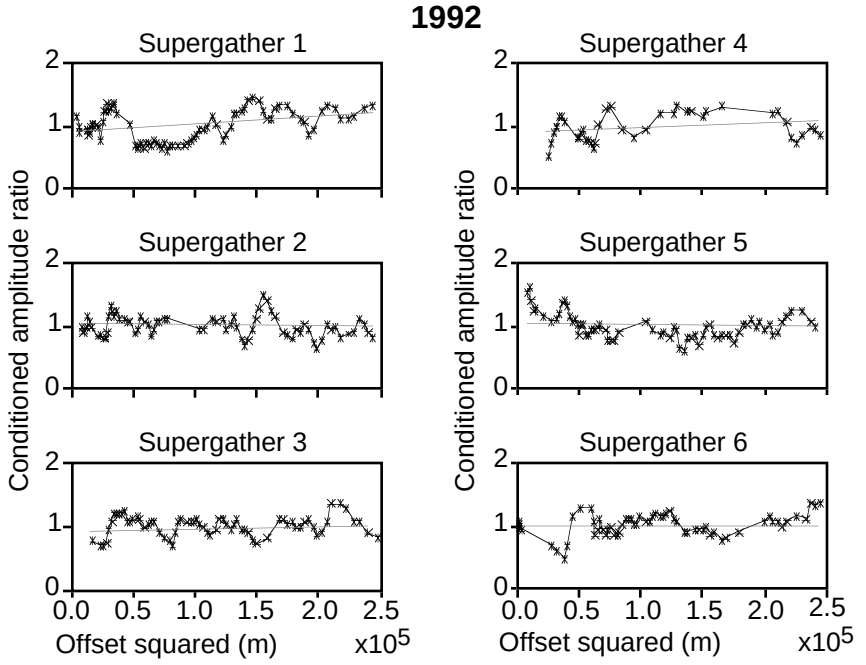

Fig. 23. Plots of conditioned amplitude ratio against offset squared for supergathers 1 to 6, extracted from the 1992 data. All offsets up to 500 m are included.

Conditioned amplitude ratios plotted against offset squared for anomalies 7 to 12, selected from the 1992 amplitude map and deep difference map displayed in Figure 15, are shown in Figures 24 and 25. The supergathers in Figure 24 were extracted from the 1992 data, in which all offsets up to 500 m were included, and those in Figure 25 from the 1990 data, in which offsets up to 250 m only were included. For supergather 7 in Figure 24 a large negative gradient is seen whereas large positive gradients occur for supergathers 8 and 10. For supergathers 9, 11 and 12 the gradient is positive, although very small in magnitude. On the corresponding 1990 supergathers in Figure 25, negative gradients are seen for numbers 9, 10, 11 and 12 and positive gradients for numbers 7 and 8.

For each of these plots in Figures 22, 23, 24 and 25, values of zero-offset intercept and gradient were extracted. The AVO difference (or "AVO") was then calculated using equation 3. These values are listed in Tables 3 and 4. The 1990 values were obtained using only the shorter offsets and an N value of 50000 was used whereas for the 1992 data, all offsets up to 500 m and an N value of 250,000 were used. Chiburis (1993) shows a model in which AVO decreases when Poisson's ratio in the target interval increases, all other parameters being constant. It might be possible to relate AVO to Poisson's ratio in the gas or steamed zone but the parameters of the overlying layer would have to remain constant. Since these low velocity intervals are found at different depths within the reservoir, the overlying layer will not always be the same one. The velocity profile of the reservoir is complicated, so to assume a constant velocity in a layer overlying the low velocity would be unrealistic.

Comments on the results from all of the twelve analysed anomalies are given below:

(1) An amplitude anomaly is absent on the 1990 amplitude map but present on the difference amplitude map. The AVO difference calculated for the 1990 data is negative but is strongly positive for the 1992 data, confirming the interpretation of an absence of gas in 1990 and the presence of steam in 1992.

(2) No anomalies exist on either map. The 1992 AVO difference value is negative and the 1990 value is positive, although very small.

(3) Anomalies are seen on both the 1990 amplitude and difference amplitude maps, indicating an absence of an anomaly in 1992. It was interpreted that a gas-saturated zone caused the anomaly in 1990. The AVO difference values are both positive. However, on the 1990 supergather in Figure 22 a large positive gradient is clearly seen while on the 1992 supergather in Figure 23 the gradient is almost flat. The strong positive gradient on the 1990 data supports the interpretation of the presence of gas in 1990. This anomaly lies in an area of higher Clearwater-Devonian interval traveltimes in 1990 than in 1992, interpreted to be caused by the presence of gas-saturated intervals in 1990.

(4) The 1990 amplitude map shows an anomaly while the difference map does not. Because of the character of the seismic data (a trough below a peak, shown in Figures 16c and 16d) it was interpreted that gas existed in 1990 and steam in 1992. The AVO differences are both positive, supporting this interpretation, although the nearest offsets are absent from the supergathers.

(5) An amplitude anomaly is observed in both the 1990 and 1992 data (displayed in Figures 16e and 16f). It was thought that gas was present in 1990 but the 1992 situation was uncertain, although the character of the anomaly indicated a tight streak rather than a low velocity zone. The positive AVO difference in 1990 and negative value in 1992 implies the presence of gas in 1990 and absence of steam in 1992.

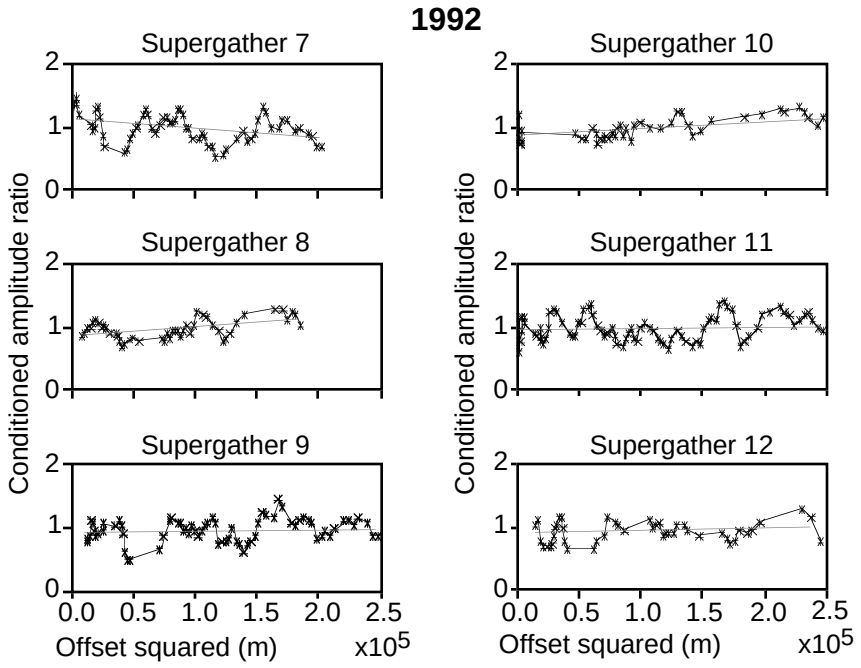

Fig. 24. Plots of conditioned amplitude ratio against offset squared for supergathers 7 to 12, extracted from the 1992 data. All offsets up to 500 m are included.

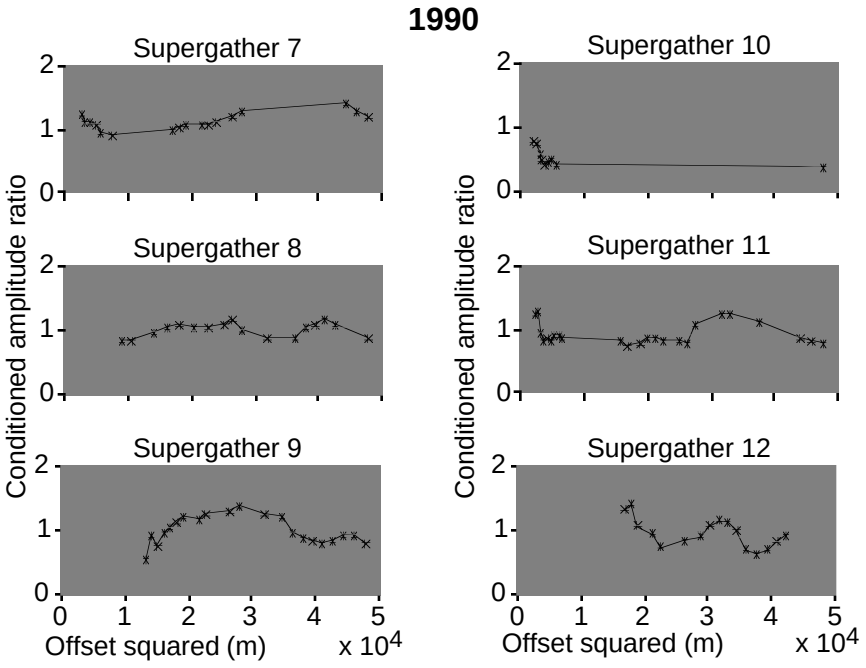

Fig. 25. Plots of conditioned amplitude ratio against offset squared for supergathers 7 to 12, extracted from the 1990 data. Offsets are limited to those below 250 m.

(6) A very strong amplitude anomaly is seen on the 1990 data and is absent on the 1992 data (Figures 16a and 16b), suggestive of a gas-saturated zone in 1990. The AVO difference is positive for the 1990 gather and negative for the 1992 gather, thus supporting the interpretation.

(7) An anomaly is absent from the 1992 data but is seen on the difference amplitude map (Figure 15), possibly due to the presence of gas in 1990. A very strong negative AVO difference is seen in the 1992 data and a positive difference in the 1990 data. This supports the interpretation of the absence of a steam anomaly in 1992 and the presence of gas in 1990.

(8) Anomalies are observed in both vintages of data (Figures 17c and 17d) and are attributed to steam zones in 1992 and gas zones in 1990. Both AVO difference values are positive.

(9) Neither of the data set exhibits an anomaly. The 1990 AVO value is negative and, although the 1992 AVO value is positive, it is very small.

(10) Anomalies appear on both the 1992 amplitude and difference amplitude maps (Figure 15) and are attributed to the presence of steam in 1992 and absence of an anomaly in 1990. This interpretation is supported by the positive AVO value for the 1992 data and the negative AVO value for the 1990 data.

(11) A strong amplitude anomaly is observed on the 1992 data but not the 1990 data (Figures 17a and 17b) and is interpreted to be caused by steam. A small positive AVO difference value is calculated for the 1992 data and a small negative AVO value for the 1990 data.

(12) Again, an anomaly exists in the 1992 data but not the 1990 data and the AVO difference values, which are positive in 1992 and negative in 1990, support the interpretation of the presence of steam in 1992.

The AVO results for the 3-D data sets analysed are summarised in Table 5. Of the 24 supergathers analysed, 21 had AVO values that agreed with the interpretation of amplitude anomalies as being caused by low velocity intervals or, for anomaly 5 in 1992, a tight streak. The negative AVO value for anomaly 5 in 1992 implies that the amplitude anomaly on the stacked data is caused by the interpreted tight streak (blue peak just above 0.42 s in Figure 16f) rather than a low velocity zone. The enhancement of this event compared with the corresponding event in the 1990 stacked data (Figure 16e) could be a tuning effect due to the presence of a lower velocity zone shallower in the section, at about 0.412 s.

The AVO analysis presented here confirms that the amplitude anomalies observed on the stacked data are due predominantly to low velocity intervals. The analysis could be taken further by pre-stack migrating both of the 3-D data volumes and sorting into 3x3 supergathers covering the whole survey. AVO analysis would be useful for confirming the spatial distribution of low velocity zones at different depths within the reservoir, as mapped from the stacked 3-D data volumes and the instantaneous frequency analysis.

Table 3. AVO difference values calculated for supergathers 1-6, chosen to analyse anomalies observed on the 1990 data at about 0.42 s.

Supergather	Intercept*1000	Gradient*1000	AVO difference
1990-1	1089	-0.00013	-0.006
1992-1	867	+0.00108	+0.366
1990-2	1168	+0.00153	+0.068
1992-2	1005	-0.00047	-0.111
1990-3	941	+0.01130	+0.684
1992-3	936	+0.00045	+0.123
1990-4	773	+0.00322	+0.206
1992-4	879	+0.00094	+0.276
1990-5	1202	+0.00955	+0.488
1992-5	1033	-0.00103	-0.233
1990-6	887	+0.00109	+0.061
1992-6	975	-0.00026	-0.066

Table 4. AVO difference values calculated for supergathers 7-12, chosen to analyse anomalies observed on the 1992 data at about 0.437 s.

Supergather	Intercept*1000	Gradient*1000	AVO difference
1992-7	1144	-0.00156	-0.341
1990-7	1065	+0.00049	+0.243
1992-8	949	+0.00148	+0.458
1990-8	948	+0.00217	+0.114
1992-9	967	+0.00007	+0.020
1990-9	1071	-0.00285	-0.133
1992-10	920	+0.00166	+0.437
1990-10	534	-0.00406	-0.368
1992-11	961	+0.00066	+0.180
1992-11	944	-0.00436	-0.232
1992-12	898	+0.00049	+0.136
1990-12	1148	-0.01553	-0.547

Table 5. Summary of AVO results for the 3-D data.

Anomaly	1990 amplitude anomaly	1992 amplitude anomaly	1990 AVO value agrees	1992 AVO value agrees
1	no	yes	yes	yes
2	no	no	no	yes
3	yes	no	yes	no
4	yes	yes	yes	yes
5	yes	yes	yes	yes
6	yes	no	yes	yes
7	yes	no	yes	yes
8	yes	yes	yes	yes
9	no	no	yes	no
10	no	yes	yes	yes
11	no	yes	yes	yes
12	no	yes	yes	yes

AVO Analysis of *P-P* 3-C data

Supergathers were formed by combining traces from three consecutive pre-stack migrated CDP gathers at selected locations along line 470-93, which is shown in Figure 25. Traces with a common offset were stacked vertically so there was a unique trace at each offset. Twenty-six gathers were selected for analysis together with a gather at the location of well BB13a on line 471-93. Sonic logs acquired at BB13a in early 1993 showed a low velocity gas-saturated zone at the top of the reservoir so a supergather was created at this location as a test case. Of the twenty-six gathers analysed along line 470-93, nine were located away from the injection wells, nine at the injection wells and eight between the injection wells.

Two events were picked interactively on each gather: a trough at the top of the Clearwater Formation and a peak representing the top of the Devonian section. Because there are far fewer tight streaks at the AABBW pads than at D3, gas, if present, is expected to be at the top of the reservoir. The top Clearwater event, therefore, was the target and was of low amplitude away from the injection wells while the Devonian event was the reference target. Rms amplitudes were extracted over a 10 ms window centred on the picked events and all offsets up to 500 m were included. The AVO values calculated by the Chiburis method for these gathers are presented in Figure 26, where the locations of steam injection wells are represented by bullets. The AVO values are negative away from the steamed zone and are positive at 7 of the 9 well locations. Between the wells, AVO values are positive at four locations and negative at four locations.

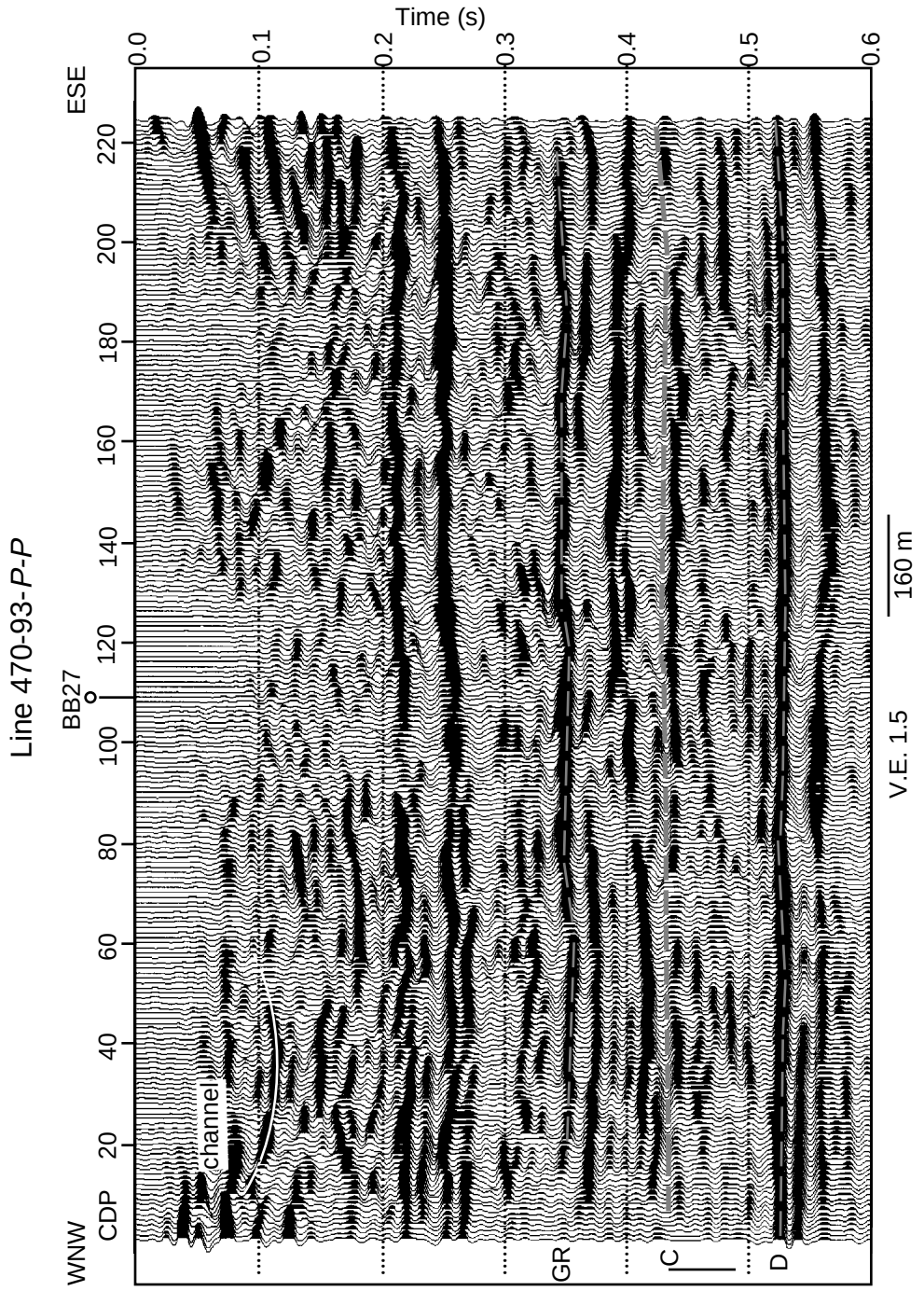

Fig. 25. Interpreted line 470-93-*P-P.* "GR" denotes the top of the Grand Rapids Formation, "C" the top of the Clearwater Formation and "D" the top of the Devonian section. The bar at the side of the sections denotes the extent of the reservoir zone.

An extremely high value is noted at an injection well location at CDP 146. A positive AVO is seen at the location of well BB13a, where 15 m of gas was present at the top of the reservoir earlier in the year.

Plots of AVO value against *Vp/Vs* at the selected locations along line 470-93 and of AVO value against scaled average amplitude along line 126-93 (the corresponding 3-D line from Imperial Oil's discriminant analysis; courtesy J. Eastwood) are displayed in Figures 27 and 28. The average amplitude values in Figure 28 were scaled so that negative values denote cold reservoir and positive values heated reservoir. All but one of the data points away from the injection wells have both a negative AVO value and *Vp/Vs* of at least 2.2. Likewise, all but one of these points have a negative AVO value and negative scaled amplitude value. From AVO value, *Vp/Vs* or absolute amplitude alone, it cannot be stated definitely that a data point lies in the cold or heated part of the reservoir. The strong correlation between AVO and *Vp/Vs* or AVO and amplitude in the cold reservoir demonstrate that, given both AVO value and *Vp/Vs* or AVO value and scaled amplitude, a data point can be classified with a higher degree of confidence. Thus AVO analysis serves as a complementary technique that could be integrated into the discriminant analysis.

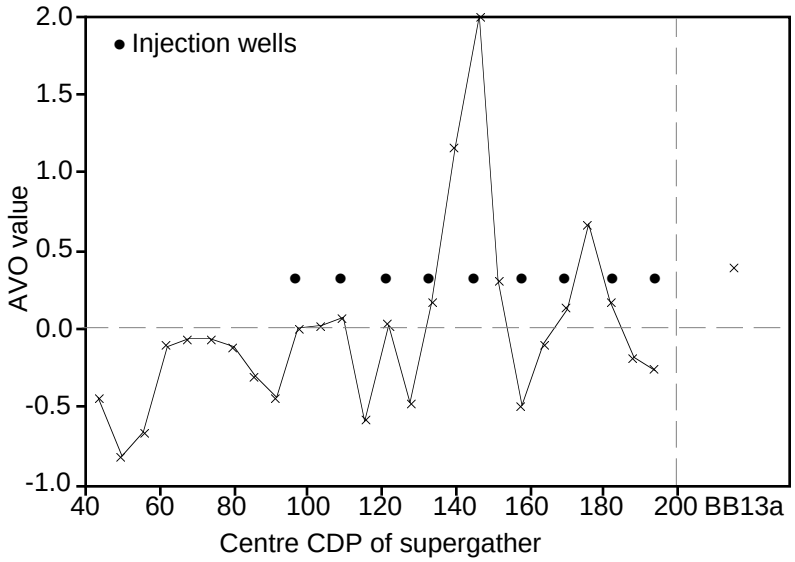

Fig. 26. Chiburis AVO values for line 470-93.

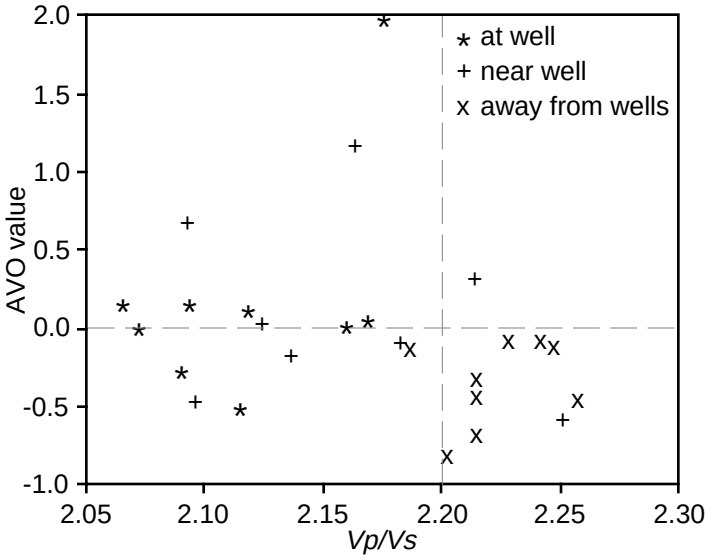

Fig. 27. Plot of AVO value against *Vp/Vs* for line 470-93.

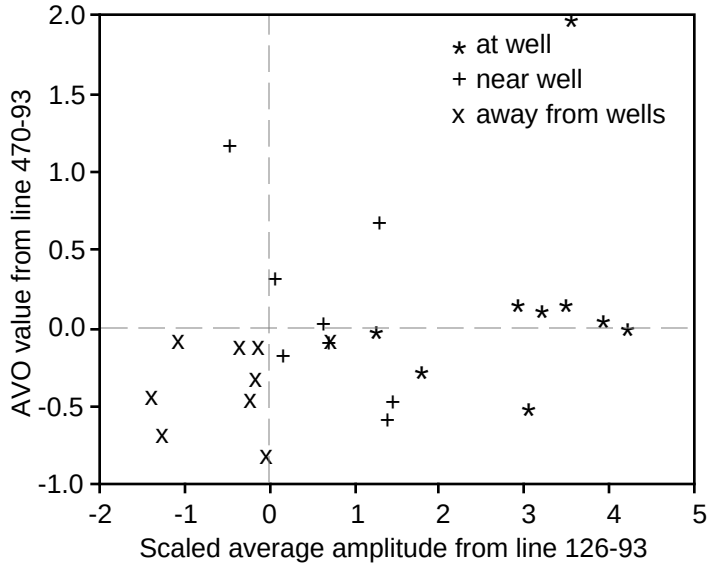

Fig. 28. Plot of AVO value for line 470-93 against scaled average amplitude for line 126-93 extracted from the 3-D survey. Values of average amplitude below zero denote cold reservoir.

DISCUSSION

The Chiburis method of AVO analysis was employed to analyse selected supergathers from the two 3-D data volumes and *P-P* line 470-93. Forward modelling of the Chiburis AVO response to be expected from low velocity zones caused by gas or steam, and the response to be expected from the chosen reference event, demonstrated that the offsets should be restricted to those below 500 m. Synthetic seismic gathers created using a wavelet extracted from the 1990 3-D data revealed ambiguous AVO responses over the offset range of 500 m. In order to discriminate between gas and no gas, offsets had to be limited to less than 250 m in the 1990 3-D data. For the 1992 3-D data and the 1993 3-C *P-P* data, the modelled Chiburis conditioned amplitude ratios showed that all offsets up to 500 m should be included in the analysis.

Amplitude anomalies were selected from the stacked 3-D data volumes and analysed. The AVO values obtained agree with the interpretation of the amplitude anomalies for 21 of the 24 supergathers examined. AVO analysis may be used to discriminate between amplitude anomalies caused by tight streaks and those caused by low velocity intervals. Analysis of selected supergathers along *P-P* line 470-93 produces negative AVO values for all the gathers away from the injection wells and positive AVO values for 7 out of 9 gathers at the well locations. Crossplots of AVO value against *Vp/Vs* for line 470-93 and against scaled average amplitude from line 126-93 indicate that a strong correlation between negative AVO value and either *Vp/Vs* over 2.2 or negative average amplitude can be used to classify that point as lying in cold reservoir. The amplitude and frequency characteristics of the seismic data are routinely analysed in detail in order to determine the extent of the heated reservoir. AVO analysis should be considered as a complementary technique whose results may be integrated with the analysis of the stacked data. The benefit of this added information is an increase in the confidence level of the classification into cold or heated reservoir.

REFERENCES

Allen, J. L. and Peddy, C. P., 1993, Amplitude variation with offset: Gulf Coast case histories: Soc. Expl. Geophys. Geophysical development series, Vol. **4**.

Chiburis, E. F., 1984, Analysis of amplitude versus offset to detect gas/oil contacts in the Arabian Gulf: 54th Ann. Internat. Mtg., Soc. Expl. Geophys., Expanded Abstracts, 669-670.

Chiburis, E. F., 1993, AVO applications in Saudi Arabia *in* Castagna, J. P. and Backus, M. M., Eds., Offset-dependent reflectivity - theory and practice of AVO analysis: Soc. Expl. Geophys. Investigations in Geophysics, Vol. **8**.

Eastwood, J., 1993, Temperature-dependent propagation of *P*- and *S*-waves in Cold Lake oil sands: Comparison of theory and experiment: Geophysics, **58**, 863-872.

Eastwood, J., Lebel, P., Dilay, A. and Blakeslee, S., 1994, Seismic monitoring of steam-based recovery of bitumen: The Leading Edge, **13**, No. 4, 242-251.

Isaac, J. H. and Lawton, D. C., 1993, Cold Lake 3-D seismic data analysis: CREWES Research Report, Vol. **5**, 25.1-25.16.

Isaac, J. H. and Lawton, D. C., 1994, 3-D and 3-C seismic data analysis at Cold Lake, Alberta: CREWES Research Report, Vol. **6**, 18.1-18.22.

Isaac, J. H. and Lawton, D. C., 1995, Converted-wave processing and interpretation at Cold Lake, Alberta: CREWES Research Report, Vol. **7**, 21.1-21.24.

Jones, I., Campbell, S. and Lancaster, S, 1995, 3D AVO processing: evolution of a processing sequence: Ann. Mtg. Can. Soc. Expl. Geophys., Calgary, Expanded Abstracts.

Ostrander, W. J., 1984, Plane-wave reflection coefficients for gas sands at nonnormal angles of incidence: Geophysics, **49**, 1637-1648.

Rutherford, S. R. and Williams, R. H., 1989, Amplitude-versus-offset variations in gas sands: Geophysics, **54,** 680-688.

Tsingas, C. and Kanasewich, E. R., 1991, Seismic reflection amplitude versus angle variations over a thermally enhanced oil recovery site: Geophysics, **56**, 292-301.

Yu, G., 1985, Offset-amplitude variation and controlled processing: Geophysics, **50**, 2697-2708.